AD-A069 048 SCIENCE APPLICATIONS INC MCLEAN VA F/G 18/8
A PROPOSED RATIONALE TO ADAPT DELFIC TO SUBSURFACE BURSTS.(U)
AUG 78 J T MCGAHAN, R J LATKO DNA001-77-C-0086
UNCLASSIFIED SAI-78-703-W/A DNA-4474F NL

1 OF 1
AD
A069 048

END
DATE
FILMED
6-79
DDC

12 LEVEL III

DNA 4474F

A PROPOSED RATIONALE TO ADAPT DELFIC TO SUBSURFACE BURSTS

Science Applications, Inc.
8400 Westpark Drive
McLean, Virginia 22101

30 August 1978

Final Report for Period January 1978—August 1978

CONTRACT No. DNA 001-77-C-0086

APPROVED FOR PUBLIC RELEASE;
DISTRIBUTION UNLIMITED.

THIS WORK SPONSORED BY THE DEFENSE NUCLEAR AGENCY
UNDER RDT&E RMSS CODE B325077464 V99QAXNA01107 H2590D.

Prepared for
Director
DEFENSE NUCLEAR AGENCY
Washington, D. C. 20305

Destroy this report when it is no longer needed. Do not return to sender.

PLEASE NOTIFY THE DEFENSE NUCLEAR AGENCY, ATTN: TISI, WASHINGTON, D.C. 20305, IF YOUR ADDRESS IS INCORRECT, IF YOU WISH TO BE DELETED FROM THE DISTRIBUTION LIST, OR IF THE ADDRESSEE IS NO LONGER EMPLOYED BY YOUR ORGANIZATION.

62704H

UNCLASSIFIED

SECURITY CLASSIFICATION OF THIS PAGE *(When Data Entered)*

REPORT DOCUMENTATION PAGE		READ INSTRUCTIONS BEFORE COMPLETING FORM
1. REPORT NUMBER DNA 4474F	2. GOVT ACCESSION NO.	3. RECIPIENT'S CATALOG NUMBER
4. TITLE *(and Subtitle)* A PROPOSED RATIONALE TO ADAPT DELFIC TO SUBSURFACE BURSTS		5. TYPE OF REPORT & PERIOD COVERED Final Report for Period January 1978—August 1978
		6. PERFORMING ORG. REPORT NUMBER SAI-78-703-WA
7. AUTHOR(s) Joseph T. McGahan Robert J. Latko		8. CONTRACT OR GRANT NUMBER(s) DNA 001-77-C-0086 new
9. PERFORMING ORGANIZATION NAME AND ADDRESS Science Applications, Inc. 8400 Westpark Drive McLean, Virginia 22101		10. PROGRAM ELEMENT, PROJECT, TASK AREA & WORK UNIT NUMBERS NWED Subtask V99QAXNA011-07
11. CONTROLLING OFFICE NAME AND ADDRESS Director Defense Nuclear Agency Washington, D.C. 20305		12. REPORT DATE 30 August 1978 13. NUMBER OF PAGES 96
14. MONITORING AGENCY NAME & ADDRESS*(if different from Controlling Office)* Chief, Livermore Branch Field Command, Defense Nuclear Agency Lawrence Livermore Laboratory P.O. Box 808, Livermore, California 94550		15. SECURITY CLASS *(of this report)* UNCLASSIFIED 15a. DECLASSIFICATION/DOWNGRADING SCHEDULE

16. DISTRIBUTION STATEMENT *(of this Report)*

Approved for public release; distribution unlimited.

17. DISTRIBUTION STATEMENT *(of the abstract entered in Block 20, if different from Report)*

18. SUPPLEMENTARY NOTES

This work sponsored by the Defense Nuclear Agency under RDT&E RMSS Code B325077464 V99QAXNA01107 H2590D.

19. KEY WORDS *(Continue on reverse side if necessary and identify by block number)*

Radioactive Fallout	Atomic Clouds
Base Surge	Depth of Bursts
DELFIC	Shallow Underground Nuclear Blasts
Vent Fraction	Activity Partition
Cloud Height	

20. ABSTRACT *(Continue on reverse side if necessary and identify by block number)*

The work reported here is intended to provide the basis for modifying the DELFIC fallout code for subsurface bursts. Models are presented for main cloud effective yield and soil loading, base surge radial growth, height and soil loading, and induced activity. The problem of using high explosive test results to supplement the nuclear data is discussed.

A

DD FORM 1 JAN 73 1473 EDITION OF 1 NOV 65 IS OBSOLETE

UNCLASSIFIED

SECURITY CLASSIFICATION OF THIS PAGE *(When Data Entered)*

TABLE OF CONTENTS

TABLE OF CONTENTS

LIST OF FIGURES

LIST OF FIGURES (cont.)

LIST OF TABLES

CONVERSION FACTORS

TO CONVERT FROM	TO	MULTIPLY BY
feet	meter	0.3048
kilotons	terrajoules	4.183
pounds	kilograms	0.4536

Section 1

INTRODUCTION

The DELFIC code is recognized in the nuclear weapon community as the DoD standard fallout model. For systems applications, other faster running codes have been devised using DELFIC calculations for calibration. The reason for the pre-eminence of DELFIC is that it includes most of the important phenomenology in greater detail than other codes. Examples include radio-chemistry, cloud rise with dependence on local humidity and temperature profiles and diffusive cloud transport. However, DELFIC does not, at present, model the phenomenology that is uniquely associated with subsurface bursts, particularly, the base surge cloud and depth of burst effects on main cloud height and activity partition between the two clouds. Hence DELFIC is not applicable for predicting fallout from Earth Penetrating Weapons (EPW) and other such weapons systems.

The objectives of this report are to investigate the fallout uniquely associated with subsurface bursts and to develop an associated model for adaptation to the DELFIC code. Section 2 is a background discussion of the phenomenology; more specifically, it addresses the current definition of initial conditions in DELFIC, development of the base surge and the impact of the ESSEX (High Explosive) results on venting of fission debris from buried bursts. Section 3 presents the modeling of the main cloud's effective yield and soil loading. Section 4 is devoted to modeling of the base surge growth and soil loading. The vent fraction and partition of activity between the main and base surge clouds is discussed in Section 5, as is the added activity resulting from neutron-activated soil. The conclusions, in the form of a summary of the work, and recommendations are given in Section 6. Finally, the appendix presents data on bulk density of the various soils in which detonations could take place.

Section 2

PHENOMENOLOGICAL BACKGROUND

In providing DELFIC with the capability for predicting fallout from subsurface nuclear detonations, there are three major phenomenological areas for which addition or modifications are required to the present code. These three areas are:

a.) modification of the main cloud initial conditions

b.) addition of a base surge cloud

c.) definition of the vent fraction of the total available radioactivity and its partition between the two clouds.

This section provides a background discussion for the analyses and model development to be reported on in subsequent sections in the context of these three phenomenology areas. In Section 2.1, the current initial conditions definition for the main cloud is examined from the point of view of identifying critical sensitivities. Section 2.2 presents a review of base surge development, summarizes the empirical relationships defining the dimensions of the stabilized base surge cloud and reviews existing models. Section 2.3 is a discussion of the implications of the ESSEX series of HE tests, which included a simulation of the venting of radioactivity.

2.1 REVIEW OF DELFIC MODELING AND ASSUMPTIONS

One objective of this work is to provide the basis for an extension of the current DELFIC code such that there is consistency in the formalism. For example, cloud rise would be treated dynamically for subsurface and surface bursts. With this in mind, then, it is appropriate to review the way DELFIC initiates cloud rise for surface bursts.

Cloud rise is treated dynamically in that mass and energy are conserved with an explicit incorporation of the relevant thermodynamics (including change of phase for water vapor). Modification of the formalism for cloud rise is not the subject here but the initial conditions which define the size and temperature of the fireball as well as its soil burden are. As will be discussed in subsequent sections, the cloud rise impacts fallout from the main cloud; the base surge will be treated separately.

DELFIC's calculated initial conditions[1] are time, temperature of the fireball gas, and soil mass and temperature. From these four parameters (as well as the ambient conditions), the code[2,3] determines the initial cloud volume, radius and height. The initial air mass is given by:

$$M_{a,i} = \frac{FW - M_r \int_{T_e}^{T_{r,i}} C_s(T)dT}{\int_{T_e}^{T_i} C_{pa}(T)dT + X_e \int_{T_e}^{T_i} C_{pw}(T)dT}$$

where W = energy yield

F = fraction of total energy for heating air and soil

M_r = soil mass

T_e = ambient temperature

$T_{r,i}$ = initial soil temperature

T_i = initial fireball gas temperature

X_e = mixing ratio (related to relative humidity)

C_{pa}, C_{pw}, C_s = specific heat for air, water vapor and soil respectively

Essentially, the above equation describes the partition of available energy for heating the air and water vapor in the cloud and the entrained soil ejected from the crater. Note that if there is too much soil or if it is heated to too high a temperature, there will not be enough energy left for air heating; in other words, the value of $M_{a,i}$ can go negative. The fireball volume is given by:

$$V_i = M_{a,i} R_a T_i^* / P$$

where

R_a = the gas constant for air
P = pressure
T_i^* = virtual temperature
$= T_i (1 + \frac{29}{18} X_e)$

The fireball shape is assumed to be that of an oblate spheroid with an eccentricity, e, equal to 0.75. The horizontal radius of the fireball is given by:

$$R = \left(\frac{3V}{4\pi} \frac{1}{\sqrt{1-e^2}} \right)^{1/3}$$

The soil loading of the cloud for surface and shallow-buried bursts is correlated with apparent crater volume as follows:

$$M_r = K_z W^{3/3.4} R^2(z) D(z)$$

where R and D are crater radius and depth for a specified scaled burst depth (in $ft/kt^{1/3.4}$) and K_z is a constant. The crater dimensions in the present version of DELFIC are appropriate only for dry soil. For 1 kt, M_r is 4.38×10^6 kg., or about 14 percent of the crater mass, M_c, i.e.,

$$M_r = 0.14 M_c$$

where each dimension of the crater scales with yield as $W^{1/3.4}$. The soil temperature in the present DELFIC Initial Conditions Module is taken to be $1000^{o}K$ with a $200^{o}K$ increase (decrease) for every decade change in yield above (below) 1 kt.

As an illustration of the above methodology, consider Jangle Uncle, a 1.2 kt shot at 17 feet depth of burst in dry soil. Two key parameters in the prediction of the fireball size are soil temperature and mass. For this shot DELFIC would calculate the soil temperature to be $1000^{o}K$ with a resulting initial cloud radius of 100 m. Shown in Figure 2.1 is the sensitivity of the initial cloud radius to variations in soil temperature and mass. Several points should be made:

a.) if the soil were at ambient temperature, the radius would have been 35 percent larger, which corresponds to a factor of two in yield.

b.) if the shot had occurred in wet soil with a substantially larger crater[4] than in dry soil, the soil burden would increase by a factor of 2.3. In that case the available energy is insufficient to heat both the soil (to $1000^{o}K$) and the air (to $2480^{o}K$). To produce a cloud of the same size as in the dry soil case, the soil temperature would have to be only $600^{o}K$. If the soil was taken to be an ambient temperature, there would be no media effect since no energy is expended in heating it.

The impact of this sensitivity to soil temperature and mass on the rise of the main cloud from a subsurface burst can only be determined by performing DELFIC calculations of observed test shots. As in the case of surface and low air bursts, soil temperature can be varied to obtain good agreement. The soil burden will be discussed in further detail in Section 3. As will be shown in Section 3, an effective yield can be determined for purposes of defining the initial conditions of the main cloud.

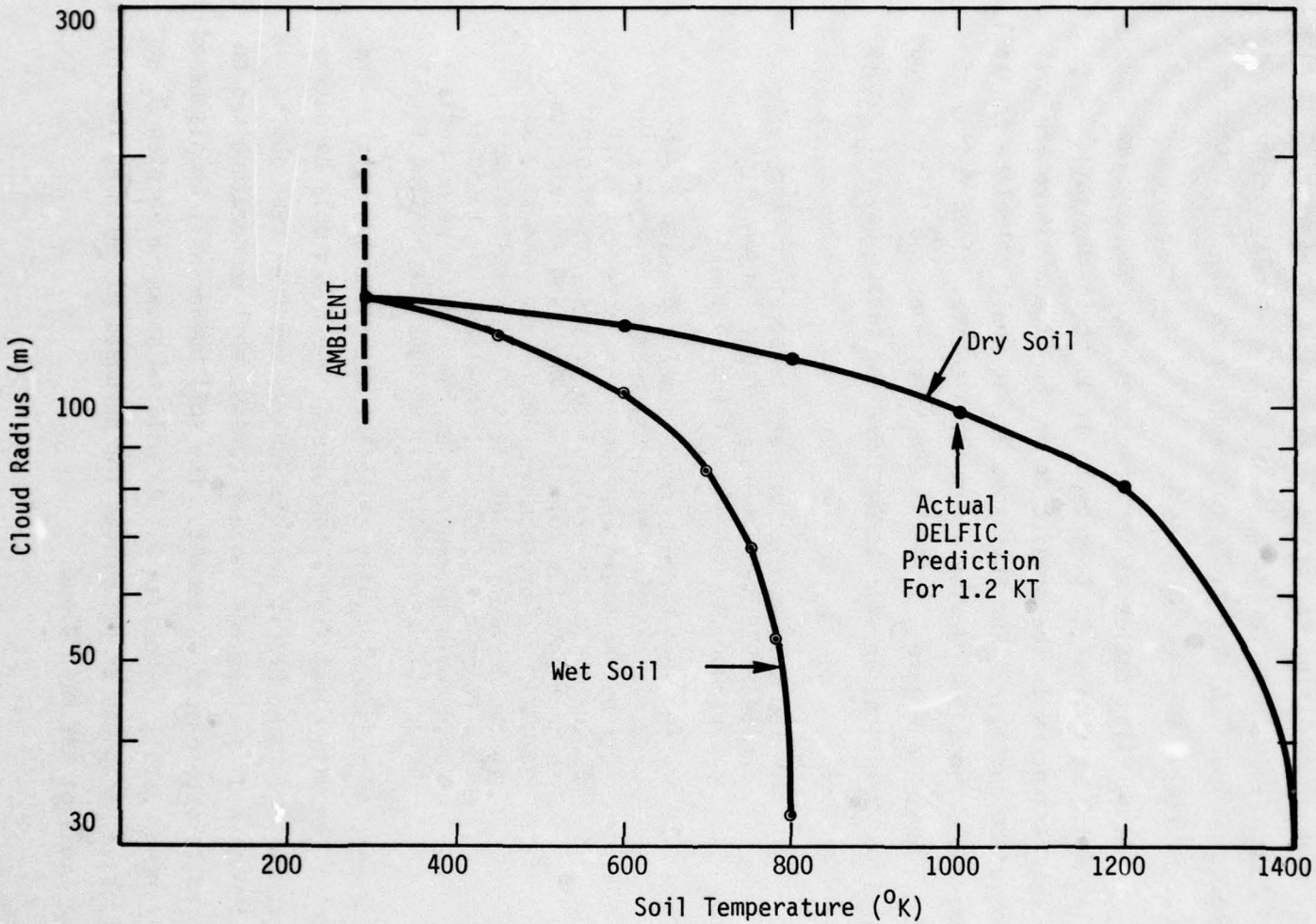

Figure 2.1. Sensitivity of Predicted Initial Cloud Radius to Soil Temperature and Mass for Jangle Uncle

2.2 BASE SURGE PHENOMENOLOGY

As an introduction to the base surge phenomenology, it is important to understand the sequence of events which lead to the formation of the base surge from a buried burst. The description presented here is based on photographic records[5] for high explosive (HE) charges detonated at one-half optimum depth-of-burial for cratering in dry clay (64.5 ft/kt$^{1/3}$). This depth-of-burial was chosen because the main features of the surface phenomena are clearly defined.

The first observable effect from an underground burst occurs when the ground shock from the detonation intersects the ground surface to form a smooth, dome-shaped mound. As the mound grows, fissures appear and the overburden material begins to break up and mix with the venting gases. The exploding mound forms a roughly spherical cloud of soil material, explosion gases and entrained air. As the smoke crown rises from the ground surface, a cylindrical column becomes visible and appears to support the smoke cloud. Shortly after the formation of the column, a high velocity jet of explosion gases breaks through the expanding smoke cloud pushing it up and out into a smoke crown. The smoke crown and jet continue to rise and expand until the initially hot gases are in local equilibrium with the ambient atmosphere forming the stabilized main cloud.

The radial growth of the column continues as the crater grows and appears to be supported by the high velocity jet which rises through the center of the column. The base surge begins to form as the crater growth stops and the entrained material in the column falls and expands radially along the ground surface. Initially, the base surge is irregular in shape and appears to be very turbulent. After the initial period of rapid growth, the base surge assumes a toroidal shape with a central depression. Throughout this period, additional material is propagated into the base surge from the smoke crown and central jet. Since this material is lighter and drops more slowly than the material in the explosion-produced column,it does not appear to have a significant effect on the radial growth of the base surge.

The base surge continues to grow vertically and radially along the ground surface until it reaches equilibrium with the surrounding air. Throughout the development of the base surge its bulk density decreases as the base surge expands and mixes with the surrounding air and the entrained soil material settles to the ground surface. As the base surge reaches its stabilized geometry, it is relatively tenuous and remains airborne for a considerable period of time.

A schematic representation of the stabilized cloud geometries that result from a buried burst are shown in Figure 2.2. Experimental evidence indicates that the relative magnitude of the stabilized clouds and the activity partition between the clouds is strongly dependent on the scaled depth-of-burst. The height of the stabilized main cloud depends on the initial energy transferred to the air and its mass loading. In general, however, the main cloud rises to an appreciable altitude and presents a serious radiological hazard at large distances from the burst point. Since the base surge cloud remains relatively close to the ground surface, a large fraction of its residual activity is expected to fall within a relatively short distance of surface zero. The final distribution of radioactive fallout depends on the features of the terrain and the local wind conditions.

2.2.1 Test Data Analysis

The initial phase of the base surge analyses was directed to collecting test data that could be used to model the formation and growth of the base surge cloud as reported in Section 4. The depth-of-burial regime of interest ranges from shallow burial (where the radius of vaporization intersects the ground surface) to the optimum depth-of-burial for crater formation.

Three nuclear tests identified as being of special interest were associated with the same type of soil (alluvium at the Nevada test site). The pertinent characteristics of these shots are presented in Table 2.1. Due to the limited number of nuclear tests, however, an

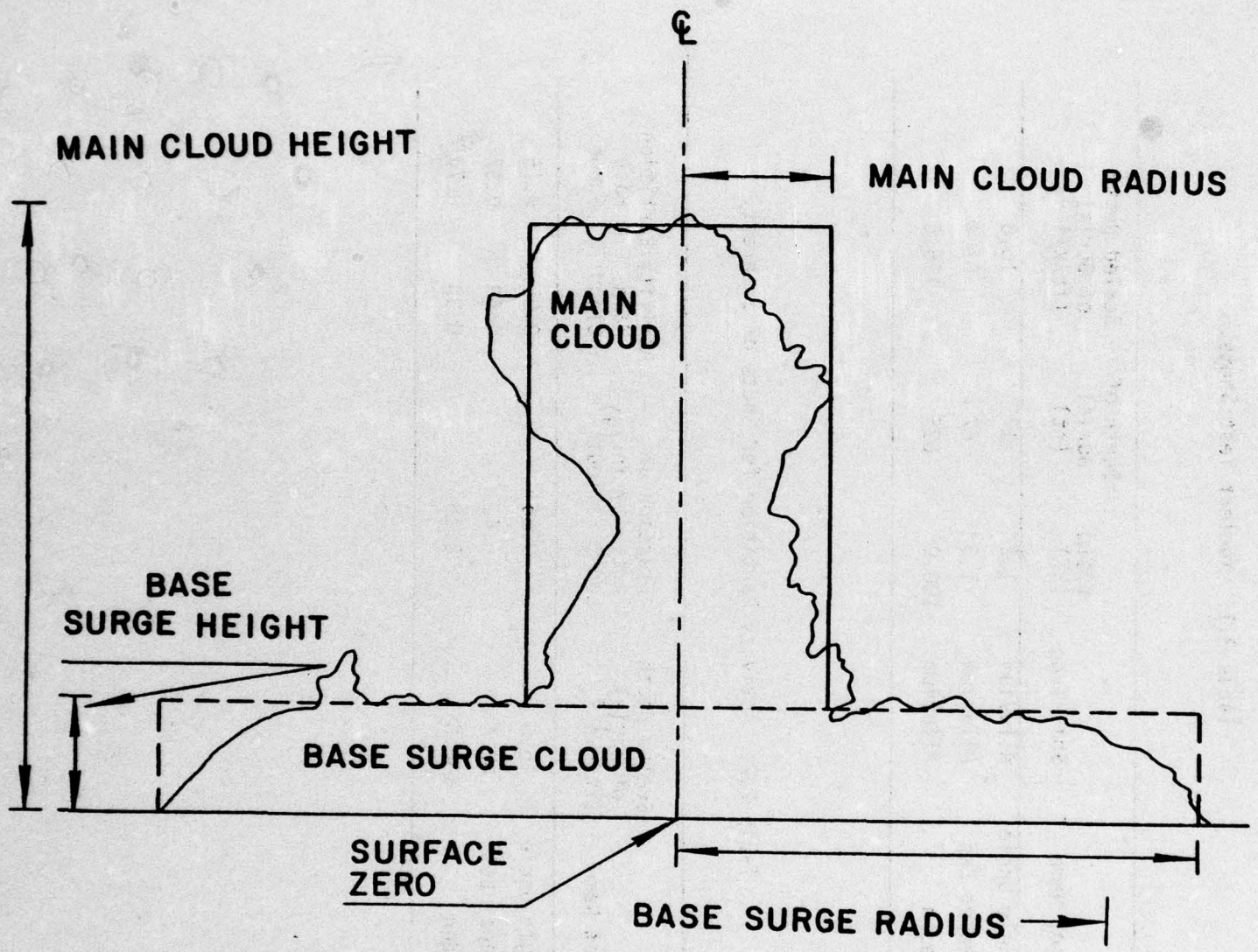

Figure 2.2. Stabilized Cloud Geometries from a Buried Burst (Extracted from Ref. 6).

Table 2.1. Nuclear Test Shots.

Shot Name	Soil Type	Yield (KT)	Depth of Burial (ft)	Scaled Depth of Burial ($ft/KT^{1/3}$)
Jangle Uncle	Alluvium	1.2	17	16.0
Teapot Ess	Alluvium	1.3	67	61.4
Sedan	Alluvium	100.0	635	136.8

Table 2.2. Activity Partition for Shots of Interest.

Shot Name	Scaled Depth of Burial ($ft/KT^{1/3}$)	Fraction of Activity in Local Fallout[9]	Activity Partition Main Cloud	Base Surge
Jangle Uncle	16.0	0.55	0.85	0.15
Teapot Ess	61.4	0.41	0.48	0.52
Sedan	136.8	0.18	0.30	0.70

attempt was made to supplement the nuclear data with HE data wherever possible. HE data were obtained for the underground explosion tests in soil at the Dugway proving ground[5] and the Jangle HE tests at the Nevada test site[5].

It is interesting to review some of the empirical relationships that have been derived from the test data. Table 2.2 indicates the distribution of the radioactivity produced by the three nuclear bursts of interest (see Section 5.2). Two important effects occur as the scaled depth-of-burial is increased: (1) the total activity in the local fallout decreases and, (2) a relatively larger fraction of the vented activity is contained in the base surge cloud. At depths-of-burial near optimum, experimental evidence indicates that a substantial fraction of the activity which escapes the crater site is carried on larger dust particles which fall within a relatively small distance of ground zero.

The scaling relationships that have been derived for the stabilized base surge cloud dimensions are shown in Figures 2.3 and 2.4[7]. It is interesting to note that the curve for alluvium is based on only three nuclear bursts in the depth-of-burial regime of interest. The only data that exist for scaled depths-of-burst greater than Sedan (137 ft/kt$^{1/3}$) were obtained from HE tests.

The reported data for alluvium and rock in Figures 2.3 and 2.4 indicate that the burst medium may play an important role in the formation of the base surge cloud. Due to the lack of data for scaled depths less than 90 ft/kt$^{1/3}$, it is impossible to construct the stabilized base surge dimensions over the entire depth-of-burial regime of interest. Additional HE data would be required in order to estimate the sensitivity of the base surge cloud to soil composition and soil moisture content.

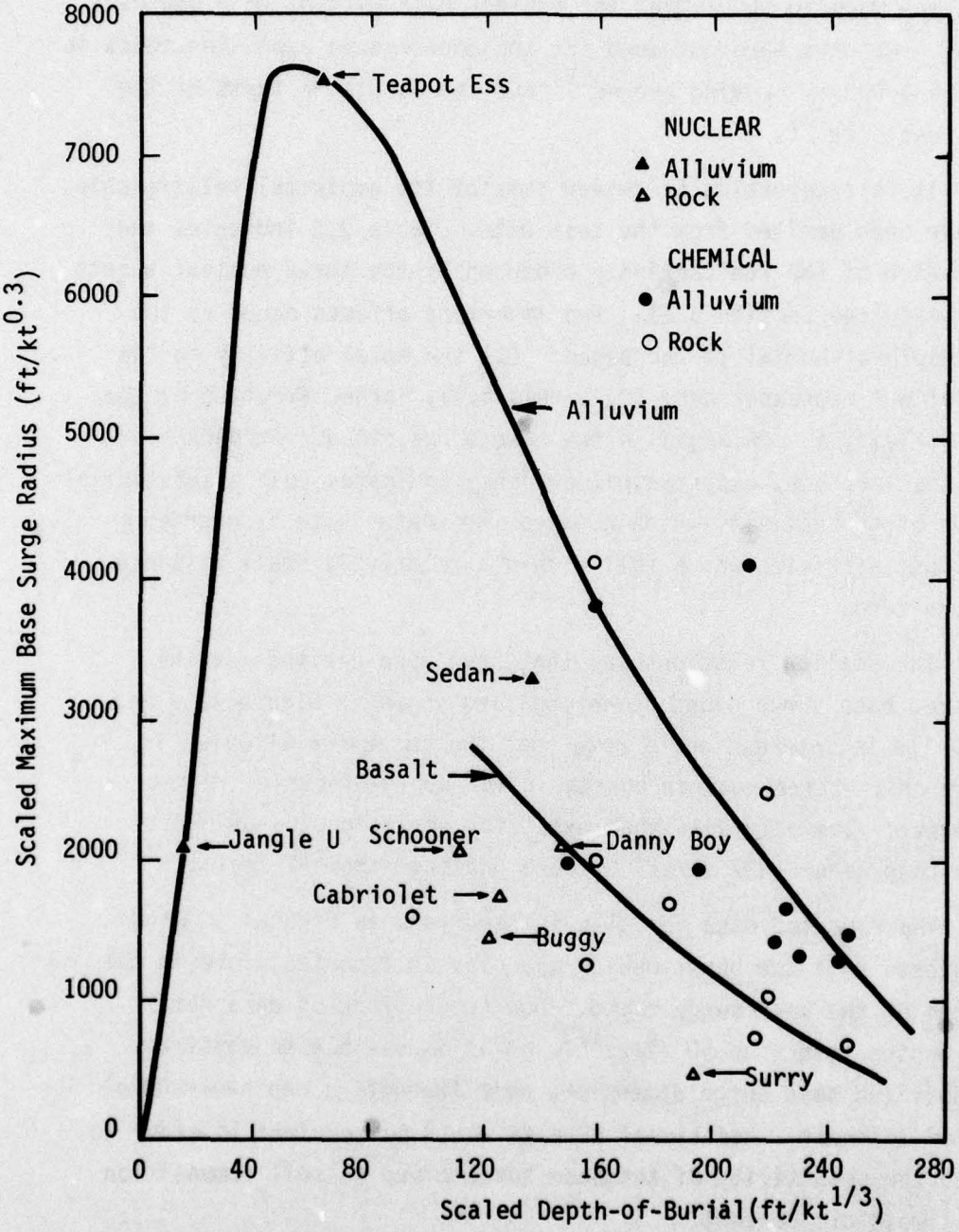

Figure 2.3. Maximum Base Surge Radius Scaled to 1 KT (Reference 7).

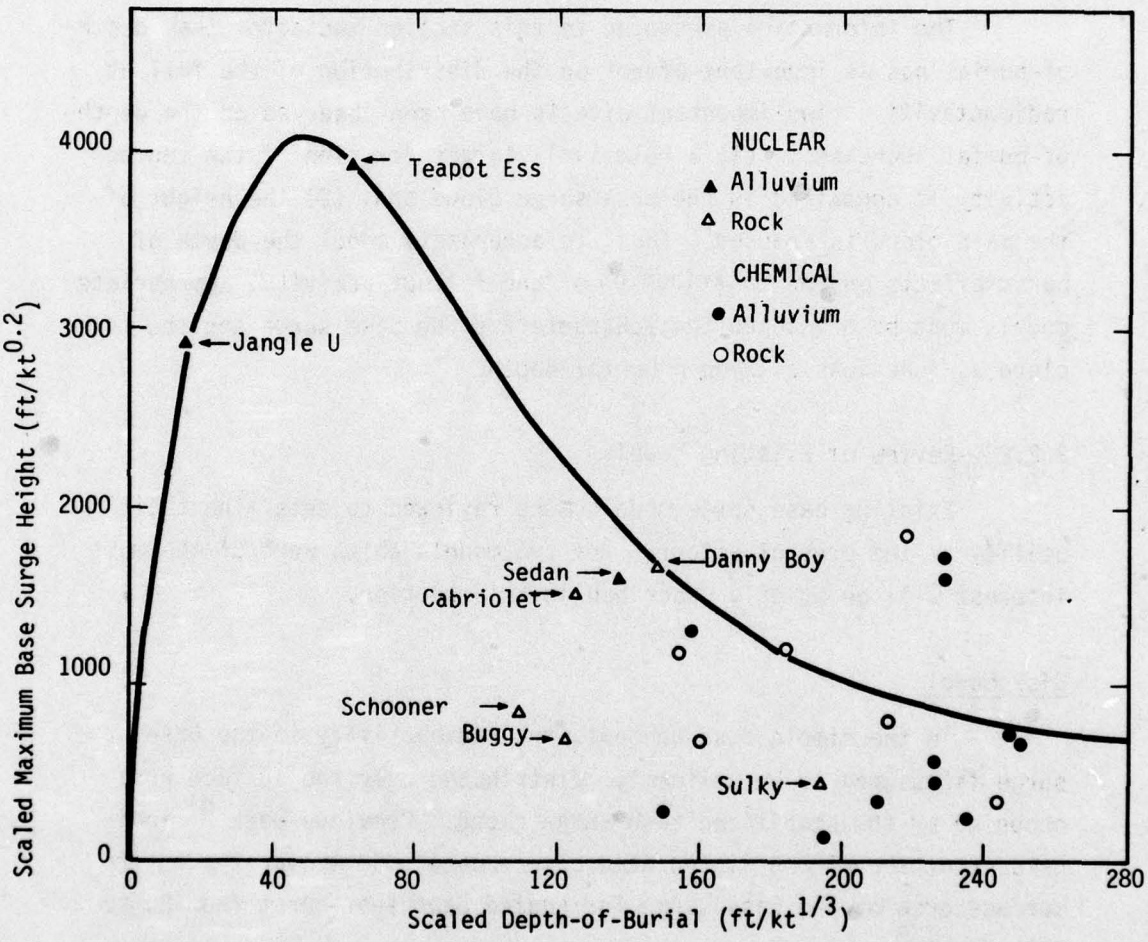

Figure 2.4. Maximum Base Surge Height Scaled to 1 KT (Reference 7).

The empirical relationship for the main cloud height is presented in Figure 2.5. It is important to note that the mean cloud height is reduced as the scaled depth of burst is increased. At the depth of burial near the optimum for cratering the main cloud height is only about 50 percent of that expected from a surface burst of the same yield.

The information presented in this section indicates that depth-of-burial has an important effect on the distribution of the fallout radioactivity. Two important effects have been observed as the depth-of-burial increases: (1) a relatively larger fraction of the vented activity is contained in the base surge cloud and, (2) the height of the main cloud is reduced. Thus, to accurately model the depth of burst effects on the distribution of the fallout activity, appropriate models must be developed that characterize the base surge and the main cloud as functions of weapon burial depth.

2.2.2 Review of Existing Models

Existing base surge models were reviewed to determine their utility to the present effort. The two models which were of the most interest will be briefly described in this section.

Disk Model

In the simple disk concept, the radioactivity in the base surge is assumed to be uniformly distributed over the surface area occupied by the stabilized base surge cloud. Previous work[8] indicates that the 24 hour integrated dose exceeds 450 R over the entire surface area of the base surge for scaled depths-of-burst from 20 to 240 $ft/kt^{1/3}$.

Test results for the measured dose rate one hour after the Teapot Ess detonation are shown in Figure 2.6. These results indicate that the measured activity is not uniformly distributed over the base surge cloud, as is assumed in the simple disk model, but that it more nearly resembles a Gaussian distribution. It has been shown[8] that the Teapot Ess activity distribution can be represented in the following form:

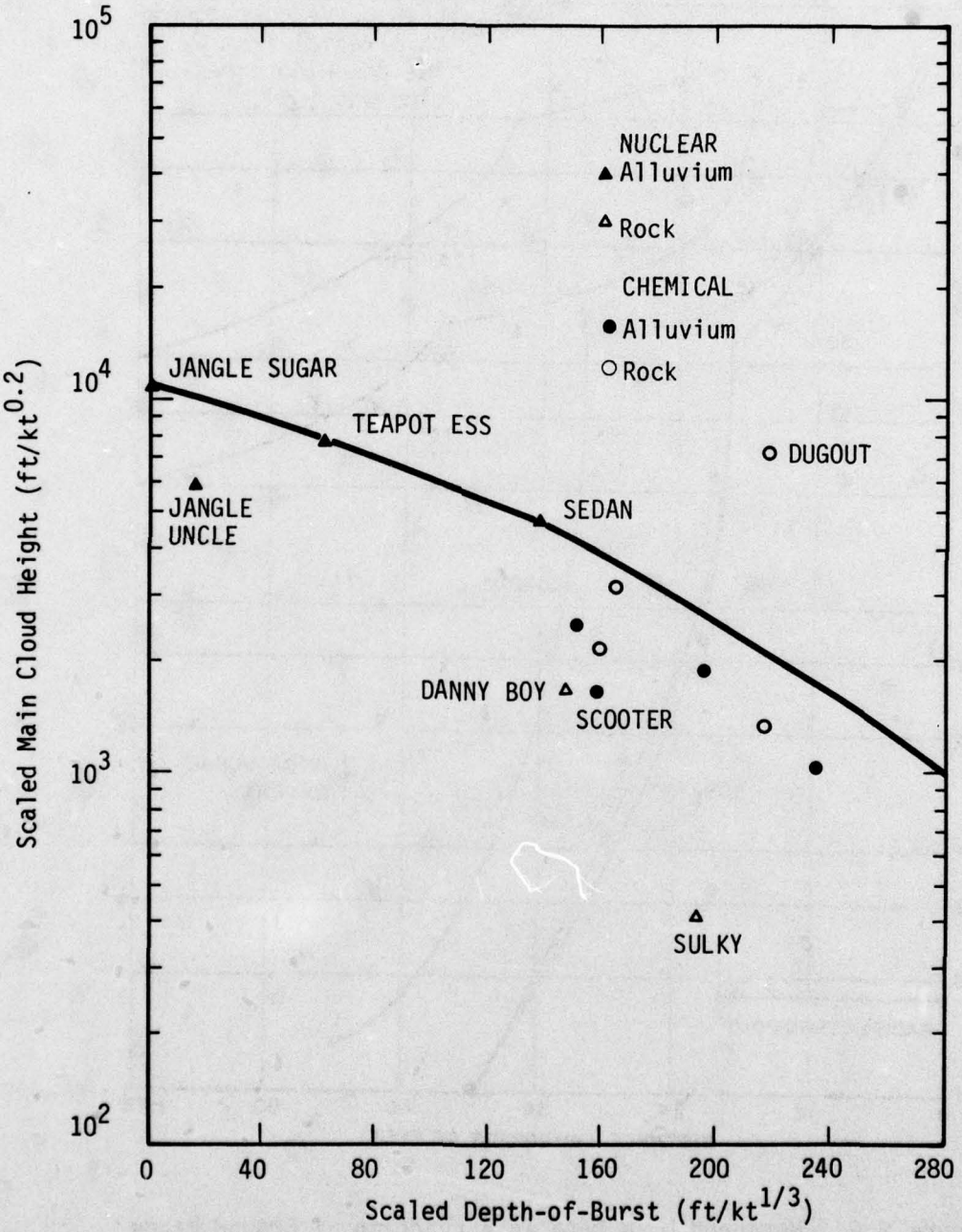

Figure 2.5. Main Cloud Top Height Scaled to 1 KT.

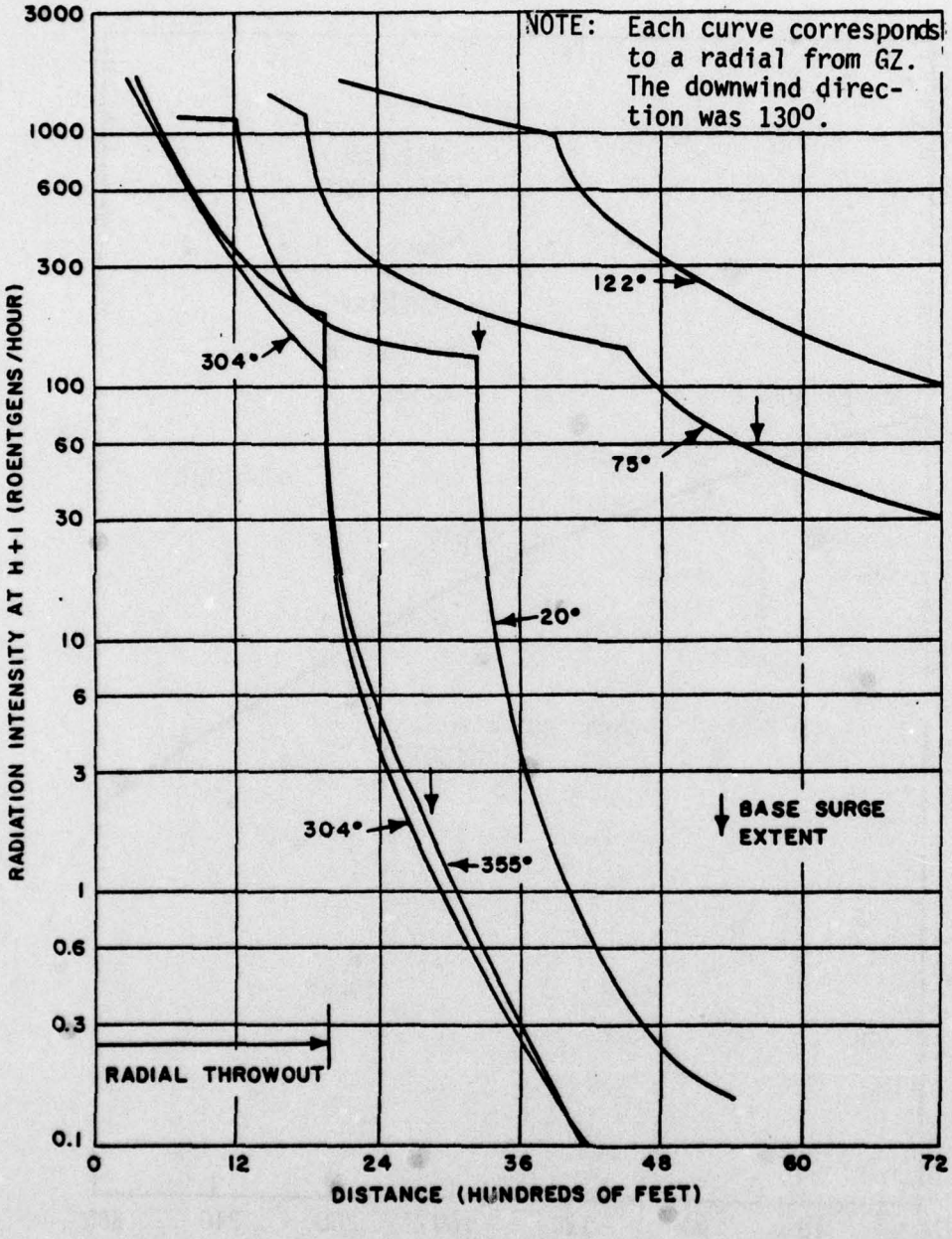

Figure 2.6. Measured Dose Rate as a Function of Ground Range One Hour After Burst for Teapot Ess[12].

$$\dot{R}(r) = 1200 \exp(-r^2/7.9)$$

where $\dot{R}(r)$ is the dose rate in R/hour and r is the ground range in Kft. Using this result, it was shown[8] that the area enclosed by the 450 R, 24 hour integrated dose contour is in excellent agreement with experimental data. A similar calculation with a uniform distribution of activity predicts an enclosed area which is 3 times larger than the measured data.

A Gaussian distribution of activity about surface zero, calibrated by experimental data, may be an adequate description of the fallout activity. An additional drawback of the disk model is that the distribution of activity on the ground surface is specified by the stabilized base surge cloud geometry independently of the surface wind conditions.

KDFOC MODEL

The KDFOC model (K Division Fallout Code) was developed by Lawrence Livermore Laboratory[9,10] for calculating the fallout from subsurface and surface nuclear bursts. Both the main cloud and the base surge are represented by their stabilized configurations as determined by fits to experimental data. Each cloud is modeled by two log normal activity/particle size distributions. One distribution applies to the entire cloud and the other to the lower one-fifth of the cloud. Each activity/particle size distribution is specified in terms of

- $\ell n\bar{r}$, natural log of the particle radius
- σ, standard deviation of the log normal distribution
- w, activity partition between the particle size distributions

The fraction of the activity produced (fission yield and equivalent yield of neutron induced radioactivity) that falls as local fallout, F_c, and the partition of this activity between the clouds is determined from empirical data. The distribution of this activity on the ground surface is obtained by subdividing each cloud into a number of subelements which are representative of the cloud height and the assumed particle size distribution. The trajectory of the centroid of each element is then determined from the terminal velocity of the particles making up the element and the wind speed acting at each altitude level through which the element falls. The final area covered by each disk on the ground surface includes the effect of lateral eddy diffusion.

The portion of the fallout pattern due to the base surge is specified in terms of the exposure rate at surface zero, $\dot{D}(SZ)$, and the radius of the stabilized base surge cloud, R(BS). The exposure rate, $\dot{D}(R)$, at a point R in this pattern is then specified by the empirical relationship

$$\dot{D}(R) = \dot{D}(SZ) \exp[-10.27\ R/R(BS)]$$

where $\dot{D}(SZ)$ and R(BS) are input quantities. Currently, the KDFOC model is calibrated by adjusting the activity/particle-size distributions in the main cloud and the base surge on a trial and error basis to force agreement with experimentally measured data.

Another model, LASEER, uses the KDFOC activity partition between main cloud and base surge but is otherwise a substantially different model. A comprehensive review of KDFOC and LASEER may be found in reference 10.

2.3 IMPLICATIONS OF ESSEX RESULTS

The series of ESSEX HE tests[11] was heavily instrumented for fallout simulation with a detailed analysis of vent fraction. This is defined as the amount of vented tracer material (iridium) deposited in the fallout pattern beyond the limit of continuous ejecta divided by the total quantity of tracer material in the charge. The results

of the analysis for a series of tests have resulted in considerable controversy because they indicate a much lower vent fraction (factor of 5) than observed in nuclear subsurface tests. This is shown in Figure 2.7. Because the ESSEX tests were in Fort Polk wet clay and the nuclear shots, by and large, occurred in alluvium, a preliminary conclusion by WES (U.S. Army Engineer Waterways Experiment Station) was that a pronounced soil dependence was evident for vent fraction and that a duplicate ESSEX test (at 6 meter depth of burst) should be conducted at a site near the nuclear tests to verify the media dependence.

The above conclusion assumes that chemical tests can be used to simulate in a consistent manner, all of the relevant fallout phenomenology associated with a nuclear subsurface burst. Intuitively, this phenomenology can be separated into two categories. The first is related to cratering; in particular the base surge cloud is directly tied to cratering. The second category is venting of the hot explosion gases; this drives the formation of the main cloud and the deposition of longer range fallout than results from the base surge. The important point is that there is no a priori reason to assume that a chemical test is a consistent simulation of both categories of the phenomenology. In other words, the fact that a nuclear equivalent yield for ESSEX has been established for cratering does not necessarily imply that this same equivalent yield applies to main cloud formation. As an illustration of this consider the 6 MS test. The assigned yield was 10 tons at a depth of burst of 19.45 ft and pre-test calculations had shown that the equivalent yield for cratering was 20 tons. On this basis, the scaled burst depth is 10 $m/kt^{1/3.4}$. The main cloud rose to a height of 0.4 km and the question is what effective yield to choose for this height. As will be shown in Section 3, the main cloud height as a function of yield, W, and scaled depth of burst, d, is given by:

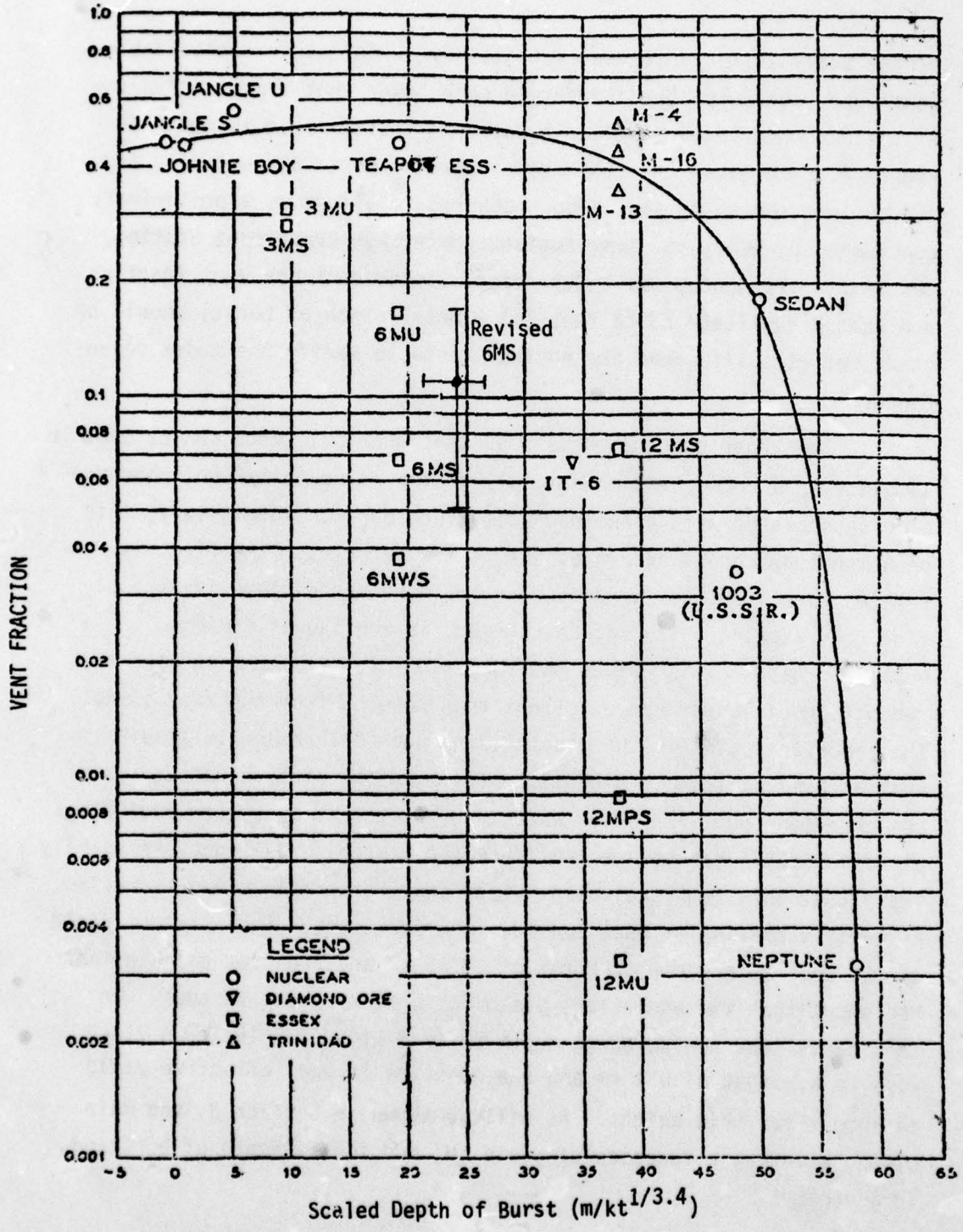

Figure 2.7. Vent Fraction Data [11]

$$H(km) = 3.4\ W^{.25} \exp\left(-\frac{d}{88.4} + 0.133\right)$$

where d is related to the actual depth of burst, D, by

$$d = DW^{-1/3}$$

Rearranging the above equation and using 0.4 km for H results in the following:

$$\ln \frac{0.4}{3.4} = 0.25 \ln W - \frac{DW^{-1/3}}{88.4} + 0.133$$

$$-2.27 = 0.25 \ln W - \frac{W^{-1/3}}{4.54}$$

The "equivalent yield" is found iteratively from this equation to be approximately 8.5 tons, which is to be compared with the 20 ton equivalent yield for cratering. From this, the scaled burst depth is 24.1 $m/kt^{1/3.4}$ (in the appropriate units for Figure 2.7). Thus the 6 MS data point should be shifted to the right by about 5 $m/kt^{1/3.4}$ as shown in Figure 2.7.

Now another shift is suggested. Recall that vent fraction is based on the amount of tracer material outside the limit of continuous ejecta. Shown in Figure 2.8 is a plot of vent fraction versus the lower range limit. For example, if the integration is started at the apparent crater radius, the vent fraction is about 0.3, compared to .07 when the limit of continuous ejecta is the beginning point of the integration. Consequently, determination of vent fraction is very sensitive to where the integration starts. While the ESSEX experiments can be assumed to have determined the limit of continuous ejecta accurately, the same cannot be assumed for the nuclear data. Consider what would happen if the 20 ton crater were replaced by one corresponding to a yield of 8.5 tons to match the size of the main cloud. If crater radius is proportional to the cube root of the yield and the continuous ejecta limit is directly proportional to crater radius, the effect is to decrease the lower range limit of the integration from 85 m to 64 m. Referring to Figure 2.8 , this means that the vent fraction increases from .068 to 0.11. The uncertainty in both

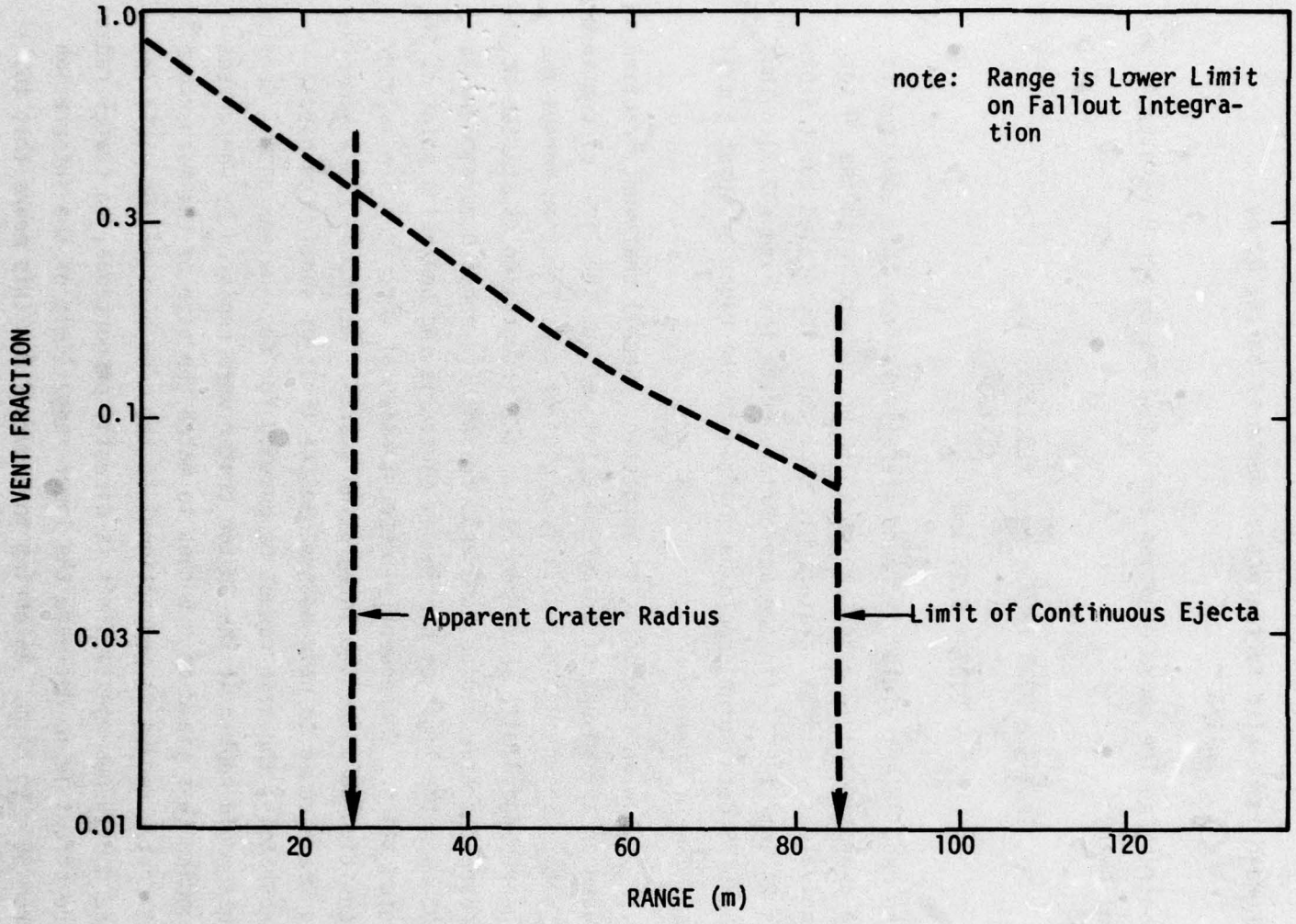

Figure 2.8. Dependence of ESSEX 6 MS Vent Fraction on Inner Range for Integration

the measurement of vent fraction and in cloud height should be considered. For the first of these, the uncertainty is estimated to be $\pm$ 50%,while a $\pm$ 25% variation is a conservative estimate for variations in cloud height. Thus the 6 MS equivalent yield for the main cloud is 8.5 $\pm$ 3.5 tons so that the scaled depth is 24 $\pm$ 2.6 m/kt$^{1/3.4}$ and the vent fraction is 0.11 $\pm$ .06. The revised location of the 6 MS data point on the vent fraction versus scaled depth of burst plot is shown in Figure 2.7. The shift is in the right direction in the sense that the discrepancy with the nuclear curve is lessened. The point of this discussion is that a full analysis of the uncertainties is required before a conclusion about soil dependence can be fully supported.

One critical aspect that is lacking in the above discussion is a comprehensive theoretical analysis of the difference between nuclear and chemical subsurface bursts. A comprehensive calculational program is required if the ESSEX tests are to be of use in developing reliable and accurate models of the nuclear phenomenology.

2.4 REFERENCES

1.) H. Norment, et al., "Dept. of Defense Land Fallout Prediction System, Vol. II, Initial Conditions," DASA-1800-II, Technical Operations Research, Sept. 1966.

2.) H. Norment, et al., "Dept. of Defense Land Fallout Prediction System, Vol. III, Cloud Rise (Revised)," DASA-1800-III (Revised) Arcon Corporation, Sept. 1970.

3.) H. Norment, "Validation and Refinement of the DELFIC Cloud Rise Module," DNA 4320F, Atmospheric Sciences Associates, January 1977.

4.) P. Dolan, ed., "Capabilities of Nuclear Weapons," Defense Nuclear Agency, (Unpublished).

5.) G. Young, "Operation Jangle, Project 1(9)-4, Base Surge Analysis - HE Tests," WT-339, U.S. Naval Ordnance Laboratory, November 1951.

6.) J. B. Knox, "Prediction of Fallout From Subsurface Nuclear Detonations," UCRL-12125 Lawrence Livermore Laboratory, Oct. 1964.

7.) W. C. Day, "Cloud Dimensions for Cratering Explosions," U.S. Army Engineer Nuclear Cratering Group, Technical Memorandum NCG/TM66-8, Sept. 1966.

8.) Nuclear Weapons Handbook for the Long Range Research and Development Program - Draft, Science Applications, Inc., Feb. 1973.

9.) J. B. Knox et al., "Radioactivity Released From Underground Nuclear Detonations: Source, Transport, Diffusion and Deposition," UCRL-50230, Rev. 1, Lawrence Livermore Laboratory, May 1967.

10.) J. B. Knox et al., "KDFOC, A Computer Program to Calculate Fallout from Underground and Land Surface Nuclear Explosions," UCRL-51179 Lawrence Livermore Laboratory, (Unpublished).

11.) J. N. Adams, "ESSEX-DIAMOND ORE RESEARCH PROGRAM: A Preliminary Assessment of the Radiation Simulation Experiments of Project ESSEX I," DNA PR0029, U.S. Army Engineer Waterways Experiment Station, Aug. 1977.

12.) M. L. Milligan and G. A. Young, "Operation Teapot - Underground Shot Base Surge Analysis," U.S. Naval Ordnance Laboratory, NAVORD Report 4153, January 1953.

13.) H. Norment, "Analysis and Comparison of Fallout Prediction Models," Atmospheric Science Associates, Bedford, Mass., March, 1977.

Section 3

MAIN CLOUD DEFINITION

3.1 EFFECTIVE YIELD

The basic assumption to be made for the main cloud from a subsurface burst is that once venting has occurred (with the resulting formation of a buoyant air mass), the subsequent cloud rise is like that of a surface burst with a reduced yield. This effective yield is reduced from that of a surface burst since more of the total energy is coupled into the ground. In DASA 1200[(1)] this problem is treated not for cloud rise but for air blast from buried bursts. The simple energy loss model is based on two assumptions:

a.) the initial explosion energy (HE or nuclear) is uniformly distributed in a sphere of radius, r_o, equal to 0.140 ft $W^{1/3}$ (lb)

b.) as the shock propagates outward, the energy loss is assumed to take place in a cylindrical tube above the burst point and that in a slice of this tube, the fractional energy loss is proportional to the mass in the slice.

Figure 3.1 is a schematic of the model. In a slice of thickness dz, then:

$$\frac{dE}{E} = - (K_1 \pi r_o^2 dz \rho)/(\frac{4}{3}\pi K_2 r_o^3)$$

where ρ is the bulk density of the soil relative to water. Combining constants and integrating results in an effective yield equal to

$$W_{eff} = W \exp(-K\rho\lambda)$$

where λ is the scaled burst depth in ft/lb$^{1/3}$. The constant K was determined to be equal to 3.0 after analysis of air blast data from subsurface bursts. This model is not quite exact in that the energy loss in the shaded portion of the tube is not handled correctly. For deep bursts this is not a problem, but for shallow bursts a modification is required. For cases where λ is less than r_o, the mass in the shaded portion is

$$\rho \frac{\pi}{3} \lambda^3$$

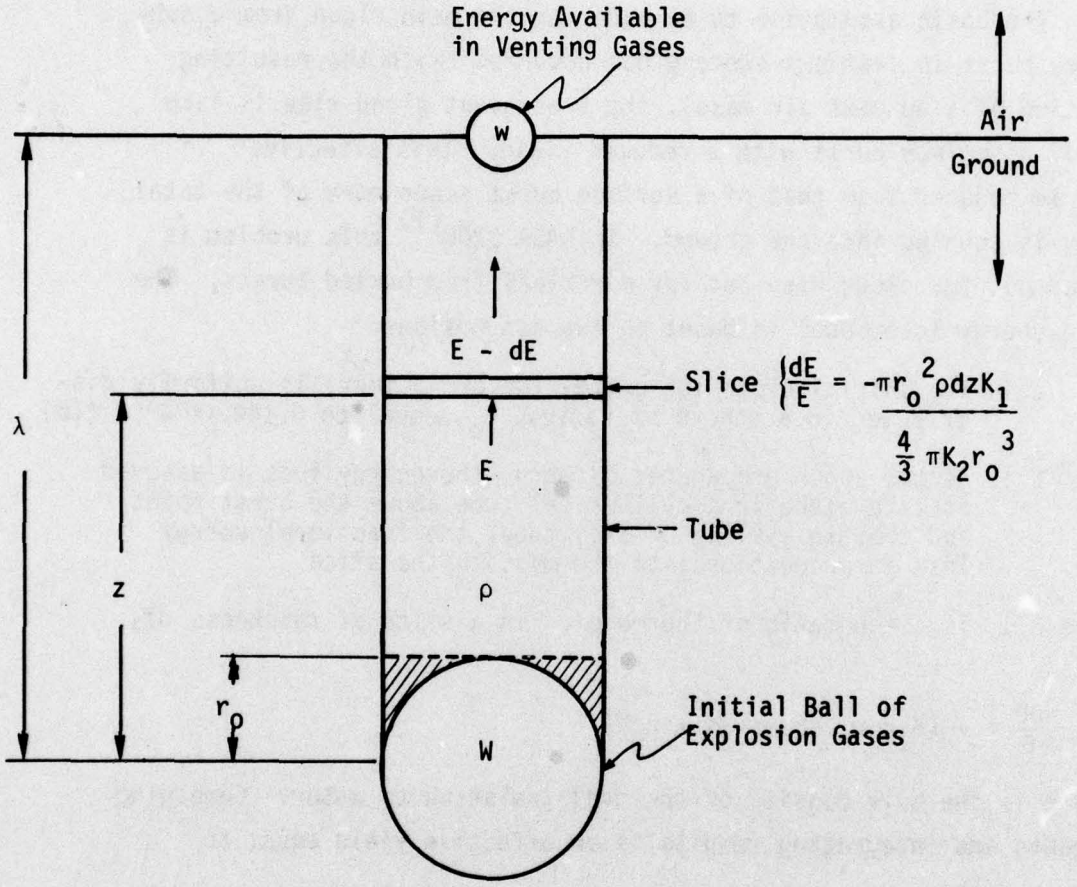

Figure 3.1. Venting Energy Loss Schematic.

The lowest-order correction, valid in the limit of small attenuation in the shaded portion, is:

$$\ln \frac{W_{eff}}{W} = \frac{-K_1\left(\frac{\pi}{3}\lambda^3\rho\right)}{\frac{4}{3}\pi r_o^3 K_2} = \frac{-K_1}{K_2}\ \frac{1}{4}\left(\frac{\lambda}{r_o}\right)^3$$

For deeper bursts:

$$\ln \frac{W_{eff}}{W} = \frac{-K_1}{K_2}\rho\ \frac{\left(\pi r_o^2 \int_{r_o}^{\lambda} dz + \frac{1}{3}\pi r_o^3\right)}{\frac{4}{3}\pi r_o^3}$$

$$= \frac{-K_1\rho}{4K_2\ r_o}\ (3\lambda - 2r_o)$$

For cases where $\lambda >> r_o$, the second term can be ignored, and the original version of the model applies so that

$$\frac{3K_1}{4K_2 r_o} = 3.0$$

For this, then, the effective yield is

$$W_{eff} = \begin{cases} W \cdot \exp\ (-\rho\lambda^3/r_o^2), & \lambda < r_o \\ W \cdot \exp\ (-3\rho\lambda + 2\rho r_o), & \lambda > r_o \end{cases}$$

As mentioned above, this model was devised for airblast from subsurface bursts. The rationale for also applying it to the initial cloud energy is that both air blast and buoyancy are due to energy transferred to air. The validity of its application here is based only on agreement with stabilized main cloud heights. By converting the scaled burst depth from λ in ft/lb$^{1/3}$ to d in ft/kt$^{1/3}$, the above equations are revised as follows:

$$W_{eff} = \begin{cases} W \cdot \exp\ (-\rho d^3/3.92\text{x}10^4) & d \leq 17.6 \\ W \cdot \exp\ \left(-\frac{\rho d}{42} + 0.28\rho\right) & d \geq 17.6 \end{cases}$$

Based on measurements of the stabilized clouds from low yield surface and low air bursts, the top height has been fitted[2] to the following expression for use in KDFOC:

$$H(km) = 3.4\ W(kt)^{0.25}$$

For a burst at depth, d, then, the cloud top height would be

$$H(W,d < 17.6) = 3.4\ W^{0.25} \exp\left[(-\rho d^3/3.92\times10^4)/4\right]$$

$$H(W,d > 17.6) = 3.4\ W^{0.25} \exp\left[\left(\frac{-\rho d}{42} + 0.28\rho\right)/4\right]$$

Since the available test data is in dry soil, the appropriate value for ρ, for comparison purposes, is assumed to be 1.9 (see Appendix). Thus

$$H(W,d < 17.6) = 3.4\ W^{0.25} \exp\left(-d^3/8.25\times10^4\right)$$

$$H(W,d > 17.6) = 3.4\ W^{0.25} \exp\left(-\frac{d}{88.4} + 0.133\right)$$

Figure 3.2 compares this model with the expressions used in KDFOC and LASEER[3] and also with limited nuclear and HE data. The principal difference with KDFOC and LASEER occurs at shallow depths of burst. The energy loss model predicts no significant decrease until the depth of burst exceeds 15 ft/kt$^{1/3}$. In wet soil, where the bulk density is lower (1.5 instead of 1.9), the predicted effective yield will be about a factor of two higher at d=100 ft/kt$^{1/3}$ with a resulting increase in the main cloud height of 25 percent. The comparison shown in Figure 3.2 indicates adequate agreement with the data. It should be emphasized, however, that DELFIC predicts cloud rise and stabilized height dynamically with explicit dependence on the meteorology rather than empirically as is the case for KDFOC and LASEER. The effective yield, determined from the energy loss model, would be used as a substitute for the total yield in the first equation of Section 2.2, i.e., the term FW is replaced by FW_{eff}.

3.2 SOIL LOADING

In line with the assumption made in the previous section, the soil loading is taken to be that of a surface burst but with a reduced effective yield. At the same time, however, there is more

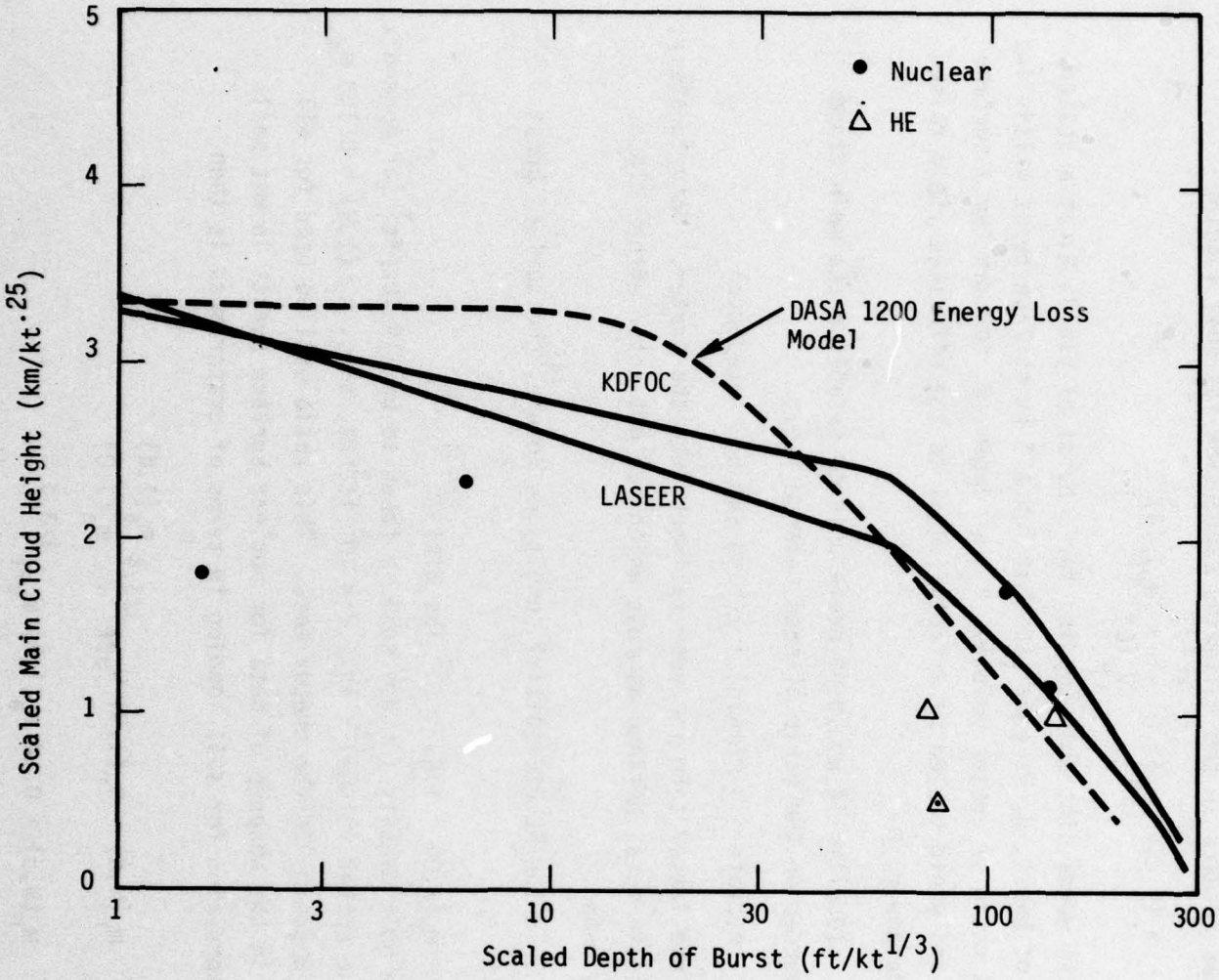

Figure 3.2. Dependence of Cloud Top Height on Depth of Burst

soil available for entrainment into the cloud due to the increase in crater volume as depth of burst increases. Combining these two premises results in the following expression for soil loading:

$$m_r(W,d) = m_r(1,0) \frac{V_a(d)}{V_a(0)} [W_{eff}(d)]^n$$

In other words, the soil loading for a burst of yield, W, at a scaled depth of burst, d, is equal to that for a 1 kt surface burst multiplied by the ratio of crater volumes, V_a, at depth, d, to that for a surface burst and yield scaled by a factor equal to the effective yield raised to some power, n.

Ideally, it would be preferable to establish the main cloud soil burden on the basis of mass balance i.e.,

$$m(\text{crater}) = m(\text{main}) + m(\text{base surge}) + m(\text{ejecta})$$

where the latter term included fallback into the crater. Unfortunately, the ejecta mass, defined as that which did not enter either cloud, is not known.

In the DELFIC Initial Conditions Module,[4] the surface burst mass is

$$m_r(W,0) = 1.99 \times 10^6 \text{ lbs } W(\text{kt})^{3/3.4}$$

If the bulk density for dry soil is taken to be 119 lbs/ft^3 (cf Appendix) and the crater volume[5] is 1.2×10^5 ft^3/kt, then, $m_r(1,0) = 0.140\ m_a(1,0)$ where m_a is the crater mass. This ratio will be used for all soils in the absence of data for nuclear surface bursts in wet soil. The expression for soil loading in terms of crater mass is then

$$m_r(W,d) = m_r(1,0)\ W_{eff}^{3/3.4} \frac{m_a(1,d)}{m_a(1,0)}$$

$$m_r(W,d) = 0.14\ m_a(1,d)\ W_{eff}^{3/3.4}$$

The effective yield, W_{eff}, was defined in the previous subsection so that

$$m_r(W,d) = 0.14\, m_a(1,d)\, W^{3/3.4} \times \begin{cases} \exp\left(-\rho d^3/4.44 \times 10^4\right), & d<17.6 \\ \exp\left(-\rho\dfrac{(d-11.8)}{47.6}\right), & d>17.6 \end{cases}$$

3.3 REFERENCES

1.) P. A. Ellis, et al., "Nuclear Weapons Blast Phenomena, Vol. III," (Unpublished).

2.) J. B. Knox et al., "Radioactivity Released from Underground Nuclear Detonations: Source, Transport, Diffusion and Deposition," Lawrence Livermore Labotatory, UCRL-50230, Rev. 2, May 1967.

3.) H. Norment, "Analysis and Comparison of Fallout Prediction Models," Atmospheric Sciences Associates, March 1977.

4.) H. Norment, et al., "Dept. of Defense Land Fallout Prediction System, Volume II, Initial Conditions," DASA-1800-II, Technical Operations Research, Sept. 1966.

5.) H. F. Cooper, "Estimates of Crater Dimensions for Near-Surface Explosions of Nuclear and High-Explosive Sources," RDA-TR-2604-001, R&D Associates, Sept. 1976.

Section 4

BASE SURGE

4.1 INTRODUCTION

This section is concerned with the physics and the methodology that are required to describe the development of the base surge cloud that is uniquely associated with a subsurface nuclear burst. Of particular interest is a description of the depth of burst effects on the distribution of the fallout activity that results from the formation and subsequent motion of the base surge cloud. The scope of the investigation is to establish simple physical models which describe the base surge phenomenology rather than the development of sophisticated numerical techniques.

Two key issues were addressed in the base surge modeling analysis:

- mass loading of the base surge cloud
- formation and growth of the base surge

As a first step in the analysis, pertinent nuclear and HE test data were reviewed and existing base surge models were studied to obtain a better understanding of the base surge phenomenology (Section 2.2). Section 4.2 describes the incompressible flow models that were developed to describe the gravity-inertial flow of the base surge cloud. Scaling relationships are derived, and the validity of the base surge models is tested against the available nuclear and HE data in Section 4.3. Based on these results, preliminary models for the mass loading and the radial growth and height of the base surge cloud are presented in Section 4.4.

4.2 BASE SURGE MODELING

The primary purpose of this analysis is to model the formation and growth of the base surge cloud as a function of weapon burial. It will be shown that simple hydrodynamic models can be developed to estimate the mass loading of the base surge cloud and to provide an approximate description of the activity/particle size distribution on the ground surface as the entrained soil material settles out from the base surge flow.

Experimental evidence indicates that the base surge cloud forms as entrained material (air, explosion gases and soil) in the explosion-produced column falls and expands radially along the ground surface. After the initial period of rapid growth, additional material is propagated into the base surge from the smoke crown and gas jet which eventually merge and form the main cloud. Since this material is lighter and falls more slowly than the explosion-produced column, it is assumed that this material does not contribute to the formation of the base surge cloud.

The basic assumption in the base surge analysis is that the entrained material in the explosion-produced column can be represented as an incompressible, homogeneous fluid (aerosol of suspended particles) with a mean density somewhat larger than the surrounding air. This assumption implies that, at least initially, the suspended particles fall at a rate substantially faster than their individual terminal velocities would indicate.

It has been shown[1] that a system of uniform sized particles can fall substantially faster than their terminal velocity in an undisturbed fluid if the particle spacing is less than about 25 particle diameters. This type of flow is induced by the cumulative entrainment of fluid which occurs as the individual particles fall. As an example, consider the motion of a spherical particle in the Stokes regime (Reynolds number <1).

Fluid is entrained by virtue of the particle's motion i.e., the fluid velocity perpendicular to the direction of motion is 41 percent of the particle's velocity at a distance of 1 particle diameter. Heavier, faster moving particles entrain additional fluid in the particle's wake. Later, it will be shown that the estimated particle spacing in the Teapot Ess column is substantially less than 25 particle diamters and, hence, the homogeneous fluid approximation is valid.

Another important assumption in the analysis is that the base surge can be represented by the flow of an incompressible fluid (constant density and volume). As the base surge expands, however, its bulk density decreases as the soil material settles out from the cloud and as air is entrained into the flow. Thus, an incompressible flow model cannot be expected to maintain all the aspects of the observed flow. It will be shown later, however, that the gravity-inertial flow model developed in this analysis is sufficient to describe a substantial portion of the radial base surge formation.

It is also assumed that the explosion-produced column can be represented by a right circular cylinder of uniform density. Experimental evidence suggests that the mass of the column is concentrated in an annulus due to the action of the high velocity jet at the center of the column. As the column collapses, however, turbulent mixing probably relaxes this assumption.

4.2.1 Similarity Solution

A similarity solution is derived for the motion at a distance from the collapse of the explosion-produced column supporting the base surge. The flow results as the potential energy of the column is converted to kinetic energy of the gravity flow. Such flows are generally referred to as gravity currents. A number of such flows have been observed and studied in nature,including turbidity currents laden with silt or sand, mud flows, avalanches and oil slicks.

The equations which describe the quasi-one-dimensional motion of a radially spreading inviscid, incompressible fluid are derived below.

Consider an annular fluid element. Conservation of mass implies that for a similar solution,

$$r^2(t)\,\delta(t) = \text{constant} \tag{4.1}$$

where r is the radius of the fluid shell, δ is its height, and t is the time. A solution for the radius of the leading edge of the surge, R_{LE}, is sought in the form

$$R_{LE}(t) = At^n$$

The scaled radius, X, invariant for a fluid element preserving similarity, is defined as

$$X = r/R_{LE}$$

Eq. 4.1 implies that the base surge height may be expressed in the form

$$\delta(X,t) = D(X)/R_{LE}^2(t)$$

Differentiation of Eq. 4.1 with respect to time yields

$$u = nXR_{LE}/t$$

where

$$u = dr/dt.$$

Conservation of momentum for the fluid shell requires that

$$\partial P/\partial r + \rho_s\, \partial u/\partial t = 0 \tag{4.2}$$

where P is the pressure and ρ_s is the density of the explosion-produced column. The pressure at any height Z within the surge, compared to that at a height Z_o outside the surge, is

$$P(X, Z, t) = P(Z_o) + (Z_o - \delta(X, t))\,\rho_o g + (\delta(X, t) - Z)\,\rho_s g$$

where ρ_o is the ambient density and g is the acceleration due to gravity.

41

Substitution into Eq. 4.2 yields

$$\rho_s XAn(n-1)t^{n-2} + (\rho_s-\rho_o)gA^{-3}t^{-3n}dD(X)/dx = 0$$

In order for the equality to hold throughout time and space, n must be 1/2 and D(X) must be of the form

$$D(X) = c_1X^2 + c_2$$

The volume of the base surge cloud, V_s, is assumed equivalent to the volume of the original explosion-produced column. Therefore

$$V_s = \int_0^1 2\pi XD(X)dX = \frac{\pi}{2} c_1 + \pi c_2$$

Another relation is required to uniquely specify c_1 and c_2. The mechanical energy equation is of no assistance, for it is identically satisfied for all c_1 and c_2. The ratio of c_1 and c_2 provides the partition (time-invariant for the similarity solution) between kinetic and potential energy. The energy partition depends on the dynamics of the column collapse, which are not represented by the similarity solution. Therefore an assumption is required to obtain a unique solution. D(0) = 0 is chosen (thus $c_2 = 0$) because it represents a reasonable starting condition for the similarity flow regime, in which the entire original column volume is assumed to be in the base surge. The coefficient A may now be determined as

$$A = 2\ [g(1 - \frac{\rho_o}{\rho_s})V_s/\pi]^{1/4}$$

The equations describing the notion of the base surge cloud are summarized as:

- Radius of the leading edge, $R_{LE}(t)$

$$R_{LE}(t) = 1.50\ [g(1 - \frac{\rho_o}{\rho_s})V_s]^{1/4}\ t^{1/2} \qquad (4.3)$$

- Velocity profile, u(X,t)

$$u(X,t) = \frac{XR_{LE}}{2t} \qquad (4.4)$$

- Thickness profile, $\delta(X,t)$

$$\delta(X,t) = \frac{0.64V_sX^2}{R^2_{LE}} \qquad (4.5)$$

If the similarity solution for the radial growth of the base surge is valid, Eq. 4.3 can be used to estimate the density and mass of the explosion-produced column, provided that the maximum dimensions of the column can be determined from experimental data. The required data have been reported for Jangle Uncle[2] and Teapot Ess[3]. For Sedan[4], the column height was taken to be the dome height[5], and the column diameter was inferred from a photograph taken at H+4 seconds.

Jangle Uncle

Jangle Uncle was a 1.2 KT burst at a depth of 17 feet in alluvium (NTS soil). Measured data were reported[2] for the radial growth of the base surge cloud, the stabilized ground zero width base surge radius, and maximum column dimensions:

- Maximum column diameter; D_{MAX} = 660 feet
- Maximum column height; H_{MAX} = 420 feet
- Stabilized ground zero width base surge radius; R_{MAX} = 2250 feet

From these dimensions the volume of the explosion-produced column was calculated as:

$$V_s = \pi(D_{MAX}/2)^2 H_{MAX} = 1.44 \times 10^8 ft^3.$$

Using this result in Eq. 4.3, the radius dependence on time for the Jangle Uncle base surge cloud becomes:

$$R_{LE}(t) = 391 (1 - \rho_o/\rho_s)^{1/4} t^{1/2} \qquad (4.6)$$

The similarity solution can be made to fit the experimental data if the effective density of the column is $\rho_s = 1.07\rho_o$. This result is shown in Figure 4.1. Because equation 4.6 has no maximum, one has to be determined. For Uncle, the radius is taken to reach its maximum value at 180 sec.

The similarity solution and the measured base surge growth are also compared in Table 4.1. It can be seen that the similarity solution is in good agreement with an average error of about 6 percent and a maximum error of 17 percent.

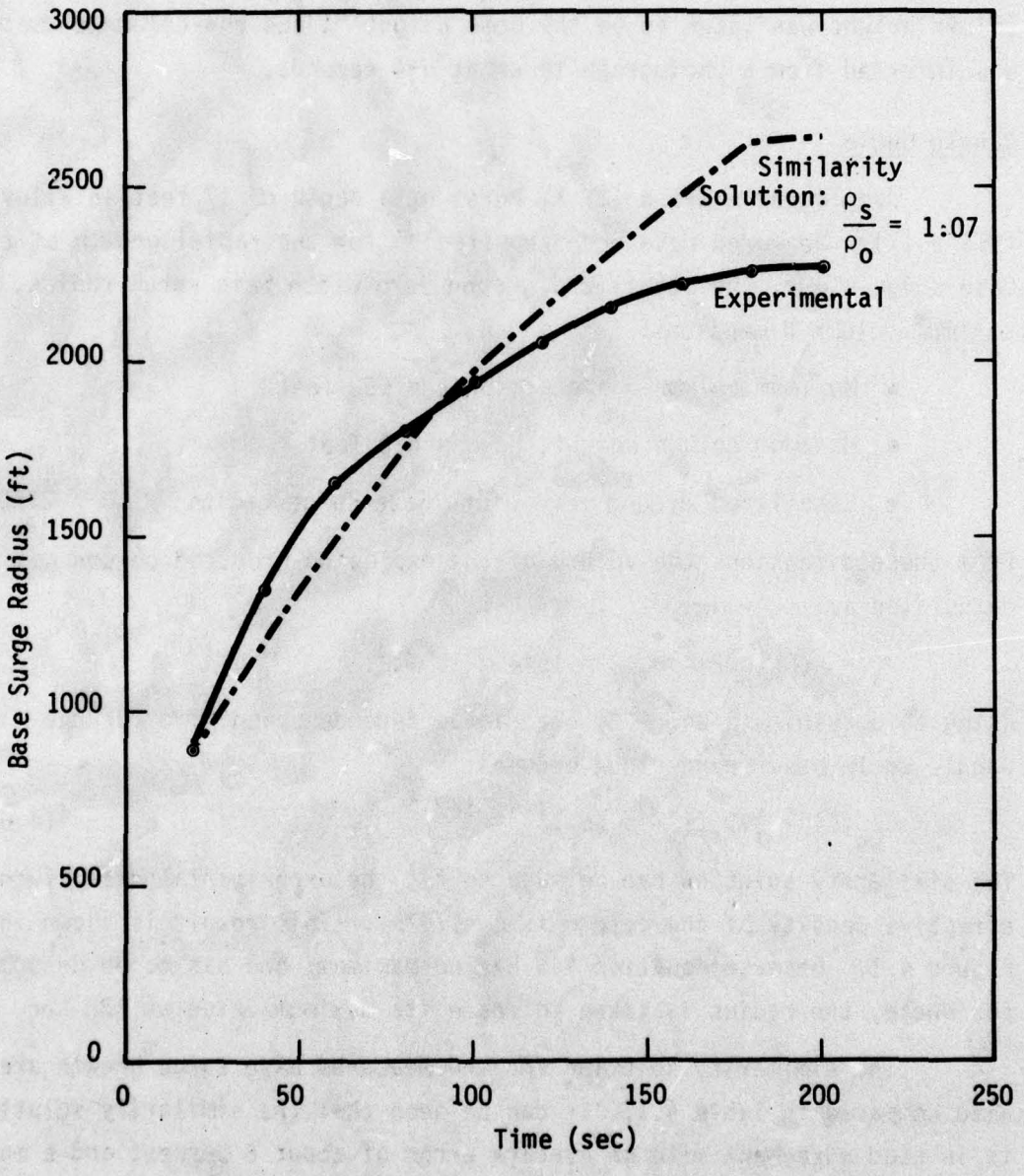

Figure 4.1. Jangle Uncle Base Surge Growth (Ground Zero Width).

Table 4.1. Jangle Uncle Base Surge Growth

Time (sec)	Measured Ground Zero Width Radius[3] (ft)	Fraction of Measured Growth	Similarity Radius (ft)	Error in Similarity Solution (%)
20	900	0.40	877	- 2.6
40	1350	0.60	1240	- 8.2
60	1650	0.73	1520	- 7.9
80	1800	0.80	1750	- 2.8
100	1950	0.87	1960	0.5
120	2050	0.91	2150	4.9
140	2150	0.96	2320	7.9
160	2200	0.98	2480	12.7
180	2250	1.00	2630	16.9
200	2250	1.00	2630	16.9

Once the effective density has been determined by matching the similarity solution and the experimental data, Eq. 4.3 can be used to estimate the effective mass of the explosion-produced column driving the base surge. The effective mass can be calculated from

$$\text{Effective mass} = \rho_o \, (\rho_s/\rho_o) V_s$$

Since the volume occupied by the soil material in the column is small compared to the total volume of the column, the mass of the soil material can be estimated from

$$\text{Soil mass} = \rho_o \, (\rho_s/\rho_o - 1) V_s \qquad (4.7)$$

Assuming that the ambient density at the Jangle Uncle site was 1.11 mg/cm^3 (ambient density at an altitude of 1 kilometer), the mass of soil in the Jangle Uncle column is estimated to be 350 tons.

Teapot Ess

Teapot Ess was a 1.3 KT burst at a depth of 67 feet in alluvium (NTS soil). The following experimental data were reported[3]:

- Maximum column diameter; D_{MAX} = 925 feet
- Maximum column height; H_{MAX} = 400 feet
- Stabilized ground zero width base surge radius; R_{MAX} = 8000 feet

The volume of the explosion-produced column is calculated to be:

$$V_s = \pi (D_{MAX}/2)^2 \, H_{MAX} = 2.7 \times 10^8 \text{ ft}^3$$

Using these data, the growth of the leading edge of the base surge cloud can be calculated from the similarity solution as follows:

$$R_{LE}(t) = 457 \, (1-\rho_o/\rho_s)^{1/4} t^{1/2} \qquad (4.8)$$

Figure 4.2 compares the experimentally measured base surge growth with Eq. 4.8 for three different density ratios, (ρ_s/ρ_o) and shows excellent agreement with the Teapot Ess base surge over the entire range of measured data. It should be noted, however, that the measured data are not complete; i.e., the ground zero width base surge radius was only measured to 6100 feet, but the stabilized radius was reported as 8000 feet. The similarity solution with $\rho_s = 2.13\ \rho_o$, which is the best fit, is compared with the measured data in Table 4.2. It can be seen that the similarity solution is in good agreement over the entire range of measured data; i.e., at least 76 percent of its final size.

Mass Loading of the Teapot Ess Column

Once the effective density of the explosion-produced column has been determined from the similarity solution, Eq. 4.7 can be used to calculate the soil loading of the Teapot Ess column. Assuming that the ambient density at the test site was 1.11 mg/cm^3, the mass in the Teapot column is estimated to be 1.1×10^4 tons.

The Teapot Ess apparent crater volume was reported to be 2.7×10^6 feet^3. Assuming an average soil density of 93 pounds/feet^3, approximately 1.25×10^5 tons of soil were permanently removed by the detonation. Based on these estimates, approximately 9 percent of the lofted soil entered the base surge cloud.

Particle Spacing in the Teapot Ess Column

A basic assumption in the development of the similarity solution is that the entrained material in the explosion-produced column can be represented as a homogeneous aerosol which falls at a rate substantially faster than the terminal velocities of the individual particles. This assumption is valid if the particle spacing is less than 25 particle diameters. Sufficient data have been derived to examine the validity of this approximation.

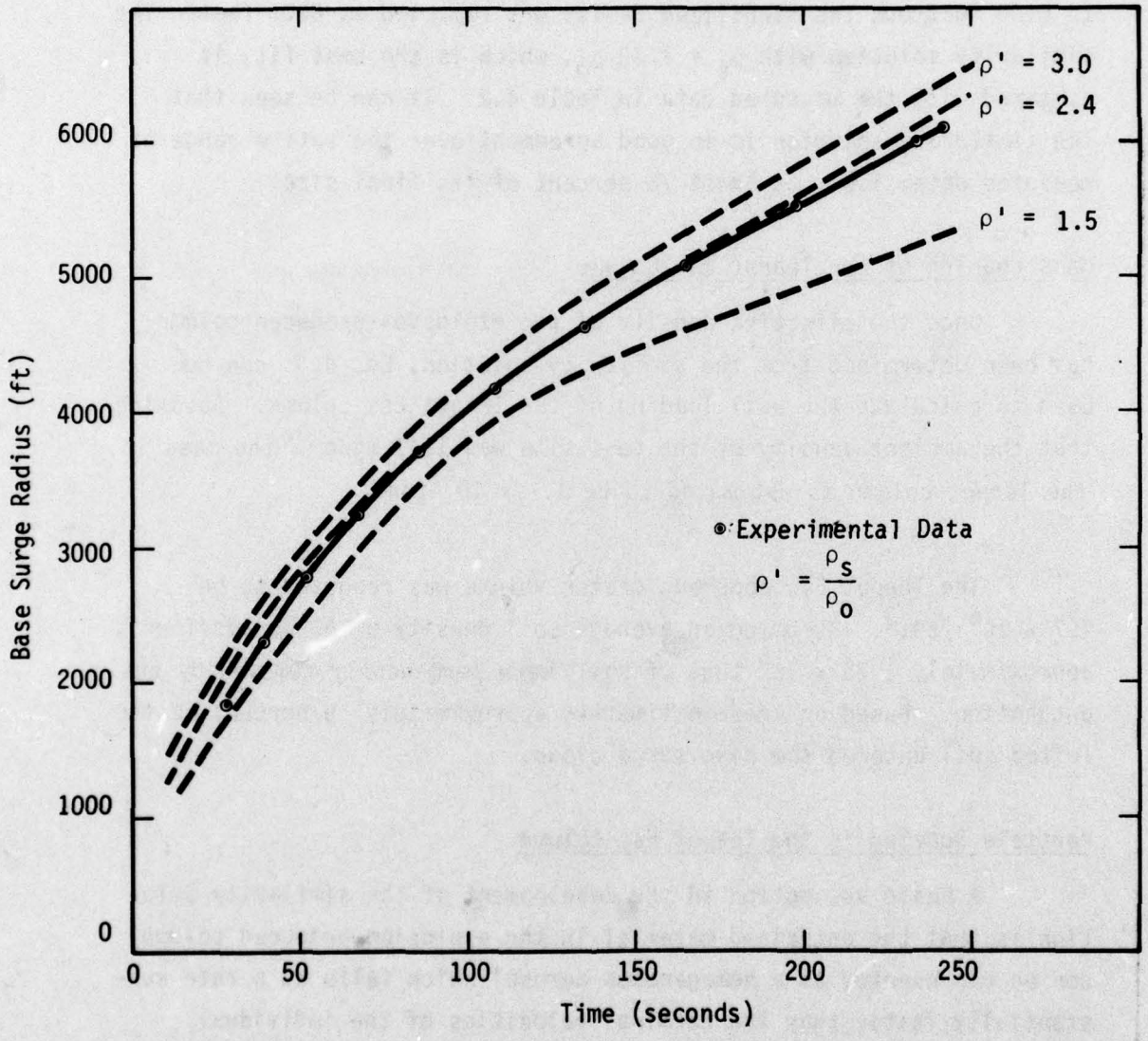

Figure 4.2. Teapot Ess Base Surge Growth (Ground Zero Width).

Table 4.2. Teapot Ess Base Surge Growth

Time (sec)	Measured Ground Zero Width Radius[3] (ft)	Fraction of Measured Growth	Similarity Radius (ft)	Error in Similarity Solution (%)
28.0	1850	0.30	2060	11
38.6	2312	0.38	2430	5.1
51.7	2775	0.45	2810	1.3
67.2	3238	0.53	3190	0
85.5	3700	0.61	3590	-3.0
108.0	4162	0.68	4050	-2.7
134.4	4625	0.76	4510	-2.5
164.5	5088	0.83	5010	-1.5
197.4	5550	0.91	5470	-1.4
233.9	6012	0.98	5960	-0.9
140.9	6105	1.00	6040	-1.1

The results of the previous analysis indicated that the Teapot Ess column contained 1.1×10^4 tons of finely divided soil material. To estimate the particle spacing, the soil mass is assumed to be made up of particles of 100μ in radius which are uniformly distributed over a volume of 2.7×10^8 feet^3. Since the average soil density was reported as 1.49 g/cm^3, each particle weighs 6.2×10^{-6} grams. The column then contains 1.7×10^5 particles (200 particles/cm^3) with an average spacing of about 8 particle diameters. Thus, the Teapot Ess column can be approximated by an aerosol of suspended particles.

Teapot Ess Similarity Model

This section presents the complete similarity solution for the development of the Teapot Ess base surge cloud. A density ratio of 2.4, not the best fit value of 2.13, was used in all the calculations. Figure 4.3 shows the position, velocity and thickness of the leading edge of the base surge cloud as a function of time. Note that the similarity solution forces the thickness of the leading edge to decrease as the base surge cloud expands. This behavior is a direct result of the incompressible fluid assumption that was used to derive the similarity solution for the radial growth of the base surge cloud; i.e., the density and volume of the base surge are constant.

The measured height of the Teapot Ess base surge cloud is shown in Figure 4.4. Clearly, the measured data are substantially different from the calculated results in all respects. Experimental results indicate that the initial base surge is very turbulent and grows rapidly in height. As the surge expands, it appears to assume a toroidal shape with a central depression. An accurate description of this aspect of the base surge flow must include some treatment of the observed vorticular motion, air entrainment and turbulent diffusion. This problem is considered in more detail in Section 4.2.2.

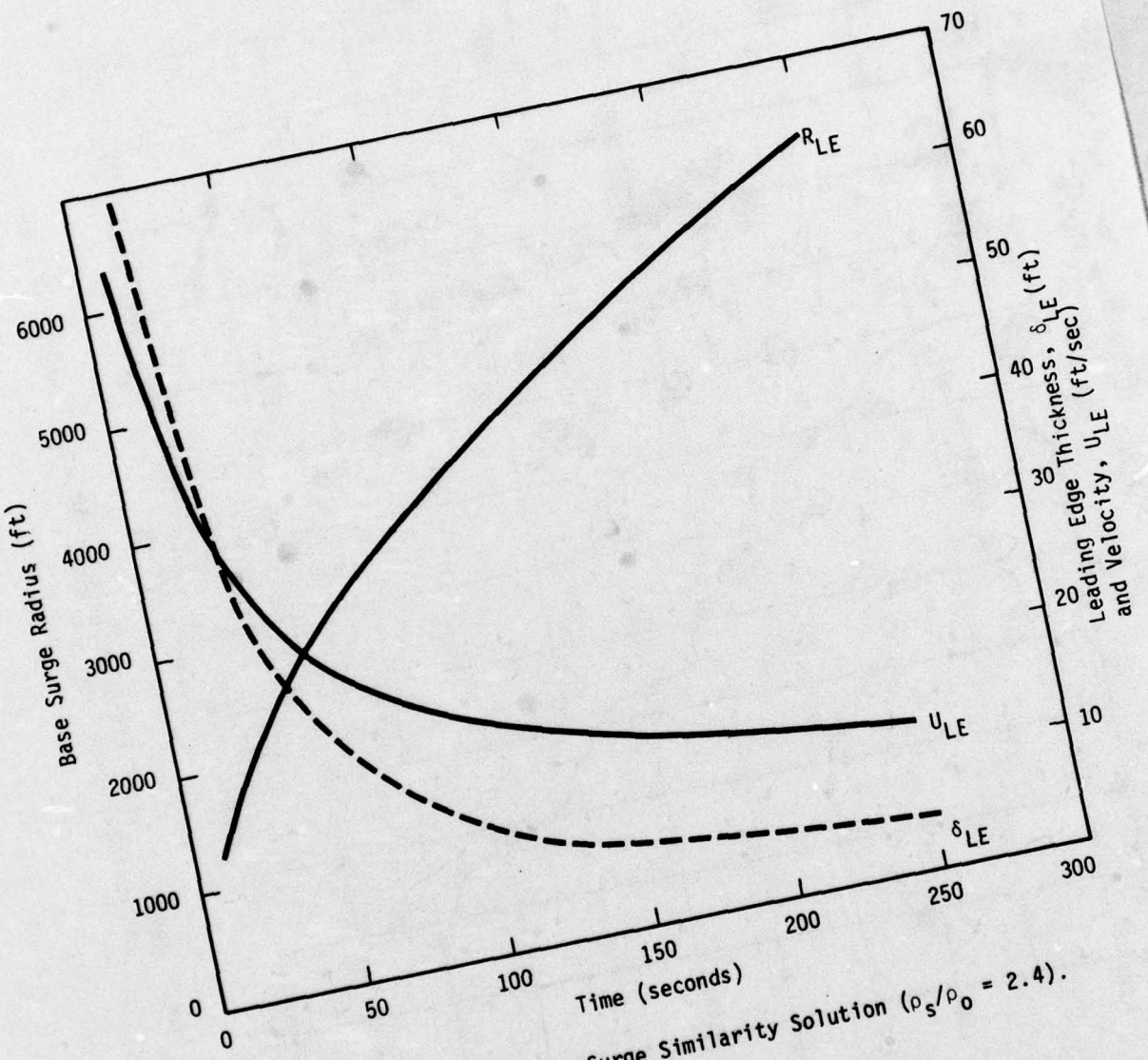

Figure 4.3. Teapot Ess Base Surge Similarity Solution ($\rho_s/\rho_o = 2.4$).

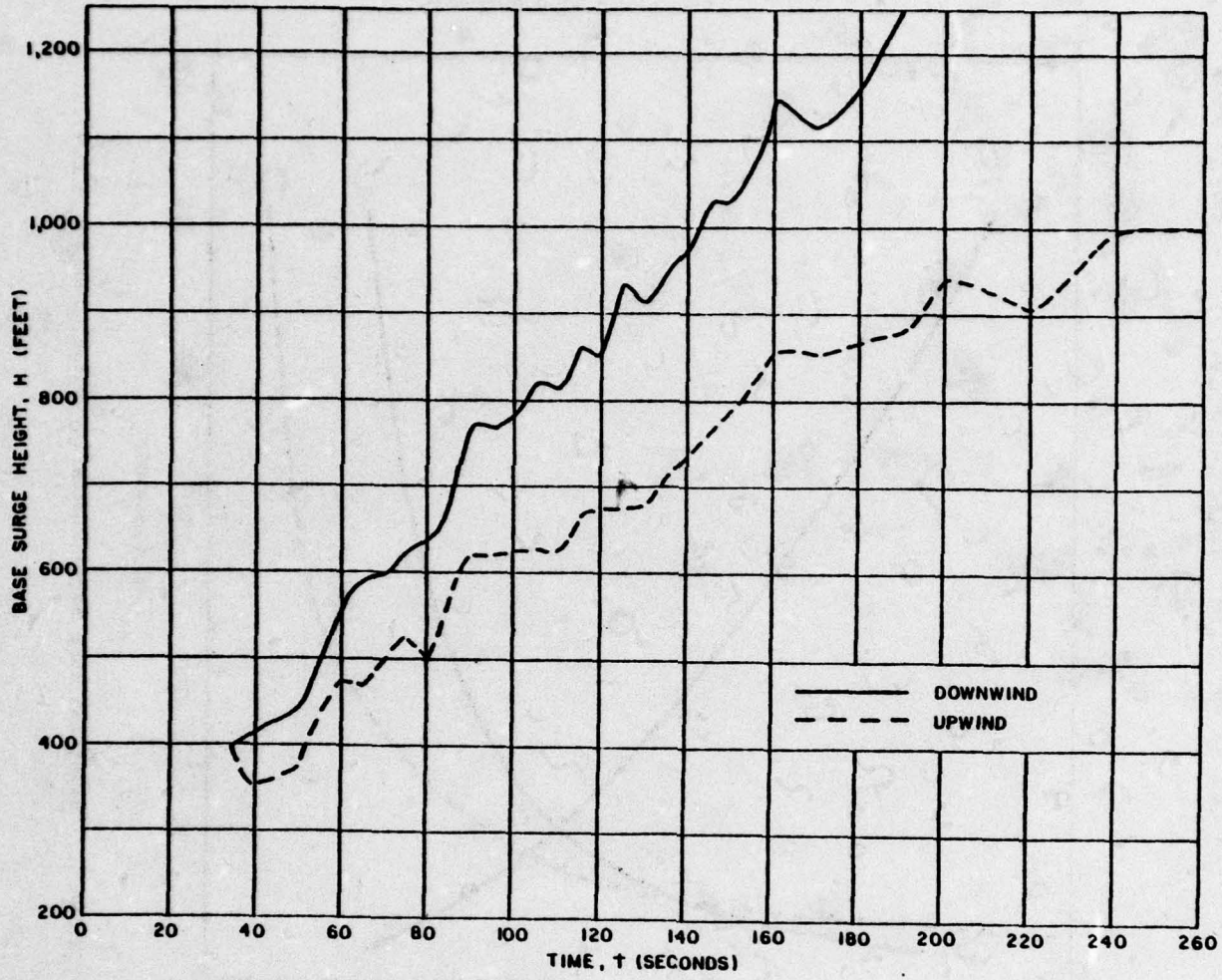

Figure 4.4. Measured Teapot Ess Base Surge Height as a Function of Time (extracted from Reference 9).

Figure 4.5 shows the similarity solution for the Teapot Ess base surge cloud at selected times. It is clear from these profiles that the similarity solution is not a good model for the early growth of the base surge cloud. Thus, it is not obvious how the similarity solution can be used to calculate the motion of the particles in the explosion-produced column to the ground surface. This difficulty can be resolved by combining the similarity solution for the radial growth of the base surge with the analytical solution for a quasi-steady gas jet impinging on a flat plate.

Sedan

This shot had a yield of 100 kt with a depth of burst of 635 ft in alluvium. The reported data for base surge development is not nearly as comprehensive as for Jangle U and Ess. As taken from reference 5, these data are

maximum base surge radius = 13,000 ft
final height = 3,940 ft
crater volume = 1.78×10^8 ft^3

Also inferred from the photographs in this reference were the column height and diameter and the surge radius at early times. The first two dimensions were based on the 4 second photograph while the radius was taken from photographs at 27, 39 and 360 seconds. This latter time was taken to be the time at which radial growth ceased. The column dimensions, then, were 1970 ft in height and 1400 ft in diameter for a volume of 3.03×10^9 ft^3. The radii, as for the previous two shots, were used to determine the density of the column to be

$$\frac{\rho_s}{\rho_o} = 2.56$$

The agreement with the measured radii is within 8 percent as shown below:

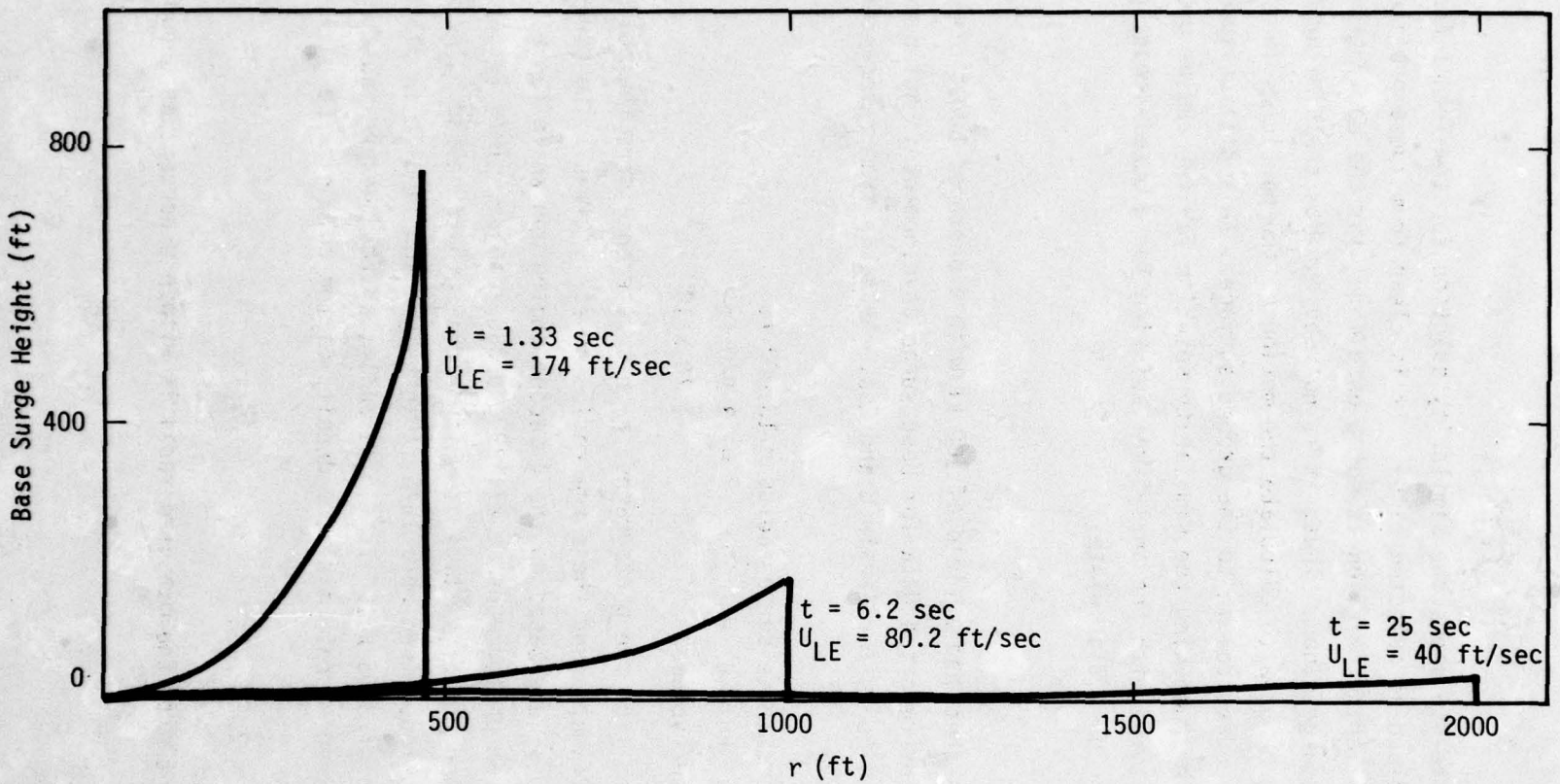

Figure 4.5. Teapot Ess Thickness Profile at Selected Times.

t (sec)	R_{meas} (ft)	R_{fit} (ft)	R_{fit}/R_{meas}
27	3700	3840	1.04
39	5000	4620	0.92
360	13,000	14,030	1.08

4.2.2 Gas Jet Impinging on a Flat Plate

The similarity solution is important in that it provides a means of estimating the mass and radial growth of the base surge cloud. One of the deficiences of the solution, however, is that it does not resemble the development of the base surge cloud at early times. Hence, another method is required to describe the particle trajectories in the base surge cloud. The analytical solution for a quasi-steady gas jet impinging on a flat plate provides the means for calculating the particle trajectories from the explosion-produced column to the ground surface.

The streamlines which define the flow of a steady, rotationally symmetric gas jet of an incompressible, inviscid fluid are given by[6]

$$r^2 z = \text{constant},$$

where the flow arrives from the z-axis and impinges on the x-y plane. The constant in the equation uniquely defines a streamline and can be evaluated at any point in the flow field. The velocity components along the streamlines are determined from the equations:

$$u = a(t)\sqrt{x^2 + y^2} = a(t)r,$$

$$v = 2a(t)z,$$

where the constant a(t) is evaluated at any point along the streamline. Since the streamlines are fixed in the flow field, a(t) can be determined from the velocity of the leading edge of the base surge cloud at any instant of time. This provides a means of calculating the time-dependent flow along each streamline in terms of the velocity and position of the leading edge as determined from either the similarity solution or experimental data.

The transport of particles from the explosion-produced column can then be calculated by solving these equations at a finite number of time steps during the development of the base surge flow. During each time step of the solution, the particles are advanced to new positions, taking into account the forces acting on the particles (viscous drag and gravitational acceleration). Since the gas jet solution is radially symmetric, the particle transport is only valid until the surface winds begin to influence the flow.

Figure 4.6 shows selected streamlines for the flow from the collapse of the Teapot Ess column. The boundary streamline is calculated by forcing the streamline to pass through the uppermost corner of the explosion-produced column.

An interesting aspect of the jet flow can be seen by calculating the bounding streamline for the Teapot Ess column. Setting $r = D_{MAX}/2$ and $z = H_{MAX}$, the bounding streamline is defined by

$$r^2 z = 8.6 \times 10^7$$

Therefore, at a time t, when the leading edge is at $R_{LE}(t)$, the thickness of the flow field can be written in terms of the above equation as

$$\delta_{LE} = \frac{8.6 \times 10^7}{R_{LE}^2}$$

Substituting $r = R_{LE}$ and $V_s = 2.7 \times 10^8$ in Eq. 4.5, the thickness of the edge given by the similarity solution becomes

$$\delta_{LE} = \frac{1.72 \times 10^8}{R_{LE}^2}$$

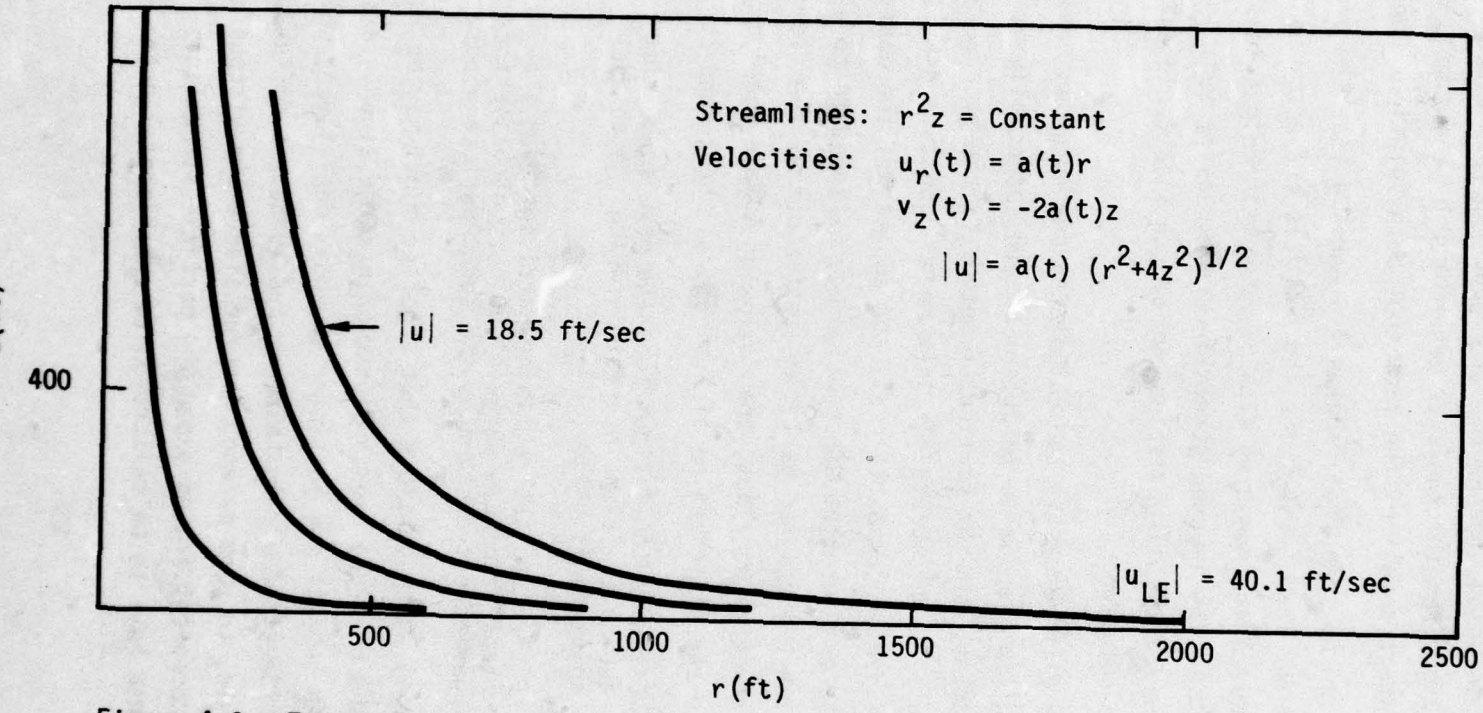

Figure 4.6. Teapot Ess Streamlines at 25 sec.

The gas jet solution, therefore, is a good representation of the particle paths and base surge thickness as determined by the similarity solution. This is a direct result of the fact that both solutions conserve mass.

It can be seen from Figures 4.6 and 4.4 that the predicted streamlines for Teapot Ess force the particle trajectories to the ground surface, whereas the measured flow increases in height as the flow expands. Thus, the imposed streamlines and gravity settling may prematurely force the soil particles out of the flow field established by the gas jet solution.

The differences in the calculated and observed behavior of the base surge flow are due to turbulent mixing (especially at early times), air entrainment, and the vorticular motion of the base surge at late times. Thus, an incompressible flow model (constant density and volume) cannot be expected to maintain all the aspects of the observed flow. However, the gas jet flow description may be adequate to estimate the rate at which the heavier particles settle out of the flow in the vicinity of surface zero. Thus, the following simple model may be sufficient to estimate the distribution of activity on the ground surface.

- Estimate the fallout from the base surge cloud during the time interval in which the gas jet solution is valid.
- Distribute the remaining particles over the stabilized base surge cloud and calculate the particle transport by the local surface winds.

It is quite possible that a better model may be required to simulate the observed growth of the base surge cloud. A simple model would be to subject the particles to additional forces which approximate the effects of air entrainment and turbulent diffusion. These forces would, to some extent, counterbalance the viscous drag and gravitational component acting along the particle streamlines. Such a formulation would have to be calibrated to experimental data.

It may also be possible to describe the base surge flow as a vortex ring impinging on a flat plate. The analytical description for this type of flow indicates that the vortex ring slows and expands radially as it approaches the plate. Such a description has not been studied in detail, but it is possible that it can be used to describe some of the main features of the observed base surge flow.

4.3 BASE SURGE SCALING

The similarity solution developed in Section 4.2.1 provides a means for scaling the base surge growth as a function of weapon burial. This is important for two reasons. First, if the scaling is valid for the depth-of-burial regime of interest, a model can be developed for the radial growth and mass loading of the base surge cloud. Second, if the nuclear and chemical data can be scaled, the nuclear data can be supplemented with a substantial body of HE data.

HE data are important because a number of tests have been performed in different soil types. Hence, it may be possible to use the HE data to determine the sensitivity of the base surge cloud to soil composition and soil moisture content. Unfortunately, the majority of the HE data that were collected for this study were incomplete, thus it was not possible to develop a detailed description of the soil dependency.

4.3.1 Scaling Relationships

Scaling relationships can be derived from the similarity solution for the radial growth of the base surge cloud. The similarity solution (from Section 4.2.1) is of the form:

$$R_{LE}(t) = 1.50 \left[g\left(1 - \frac{\rho_o}{\rho_s}\right)V_s\right]^{1/4} t^{1/2}$$

where V_s is the volume of the explosion-produced column creating the base surge. Defining a characteristic length, $L = V_s^{1/3}$, Eq. 4.3 can be written in the form:

$$\frac{R_{LE}(t)}{L} = K\left(1 - \frac{\rho_o}{\rho_s}\right)^{\frac{1}{4}} \frac{t^{\frac{1}{2}}}{L^{\frac{1}{4}}}$$

where K is a constant of proportionality.

It should be possible, therefore, to scale the radial growth of the base surge cloud by the following variables:

$$R^* = \frac{R_{LE}(t)}{V_s^{1/3}} , \tag{4.9}$$

and

$$t^* = (1 - \frac{\rho_o}{\rho_s})^{1/2} \frac{t}{V_s^{1/6}} \tag{4.10}$$

If these scaling laws are valid, experimental data for the scaled radial growth of the base surge cloud for bursts at different scaled depths-of-burial should fall on the same curve.

Figure 4.7 shows the scaled experimental results for Jangle Uncle and Teapot Ess. The results are in good agreement up to a scaled time of about 3 sec/feet$^{1/2}$, which corresponds to a real time of about 90 sec for Jangle Uncle. At this time approximately 90 percent of the final Jangle Uncle base surge growth has been completed.

4.3.2 HE Scaling

The purpose of this analysis was to examine the effect of charge weight on the scaling relationships and to determine if the nuclear and HE data could be scaled. A constant scaled depth-of-burial of 64.5 feet/KT$^{1/3}$ was chosen such that the HE data could be compared to Teapot Ess. Results are presented for charge weights of 320, 2560,

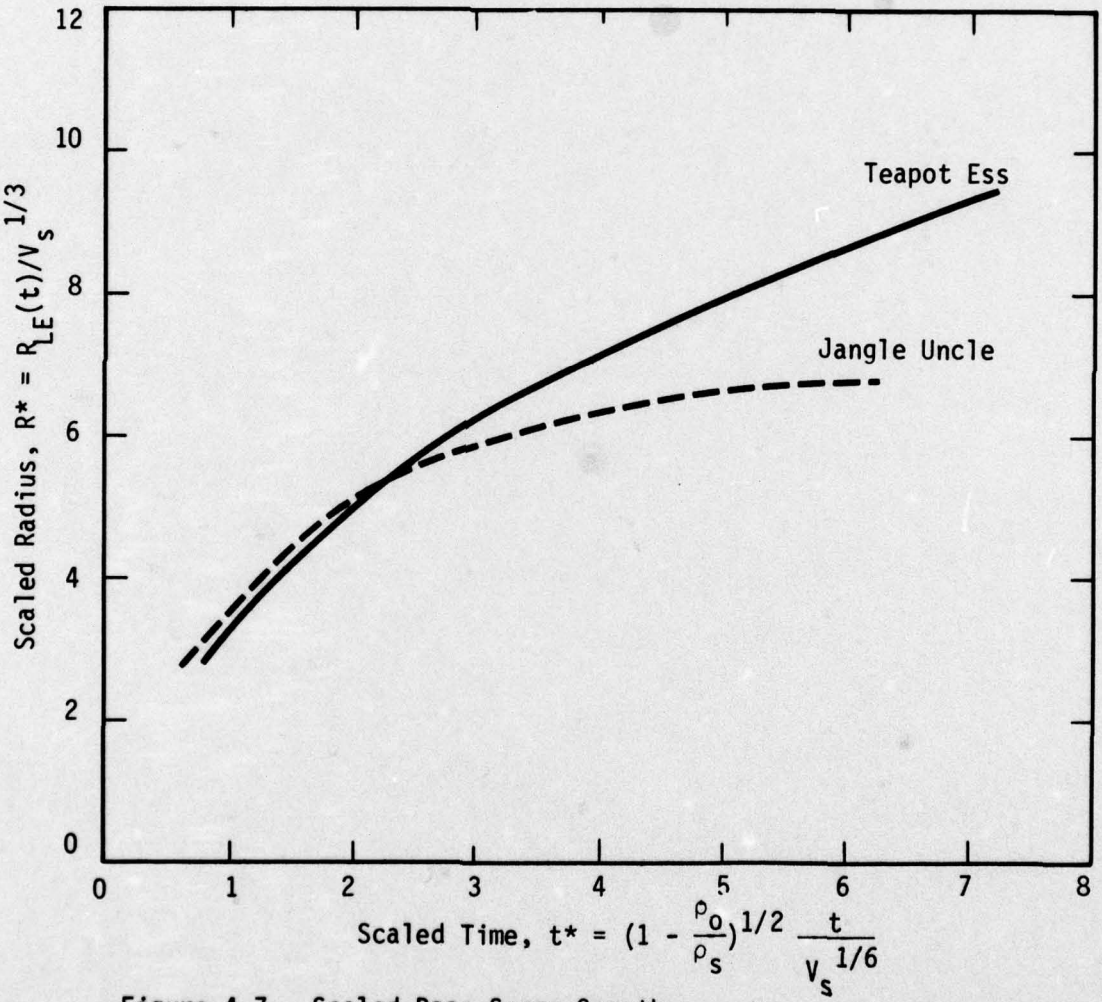

Figure 4.7. Scaled Base Surge Growth

4000 and 32,000 pounds of TNT. The HE charges were detonated in dry clay at the Dugway Proving Ground[7] (seismic velocity, 2500-3000 fps). Teapot Ess was detonated in alluvium at the Nevada test site (seismic velocity, 3000 fps). Since the soils at the two sites have the same general characteristics, it was hoped that the radial growth of the base surge was similar for both the nuclear and HE charges.

The following assumptions were made in developing the scaling relationships for the constant scaled depth-of-burial case:

- the column dimensions are proportional to charge weight
- the effective density of the explosion-produced column is constant
- the volume of the explosion-produced column, V_s is proportional to the apparent crater volume, V_a

The last assumption can be written in the form:

$$V_s \propto R_a^2 D_a$$

where R_a and D_a are the apparent crater radius and crater depth, respectively. For a fixed depth-of-burial[10],

$$R_a \propto W^{0.3},$$

$$D_a \propto W^{0.3},$$

and, hence,

$$V_s \propto W^{0.9}$$

Using these results, the scaling relationships given in Eqs. 4.9 and 4.10 can be written as

$$R^* = \frac{R_{LE}(t)}{V_s^{1/3}} = \frac{R_{LE}(t)}{W^{0.3}} \quad ,$$

and

$$t^* \propto \frac{t}{V_s^{1/6}} \propto \frac{t}{W^{0.15}} \quad .$$

The constant of proportionality may be disregarded for comparisons involving nonvarying soil density.

The scaled data for the HE charges and Teapot Ess are shown in Figure 4.8. Except for the 320 pound charge, it can be seen that the scaled data are in excellent agreement up to a scaled time of about 20

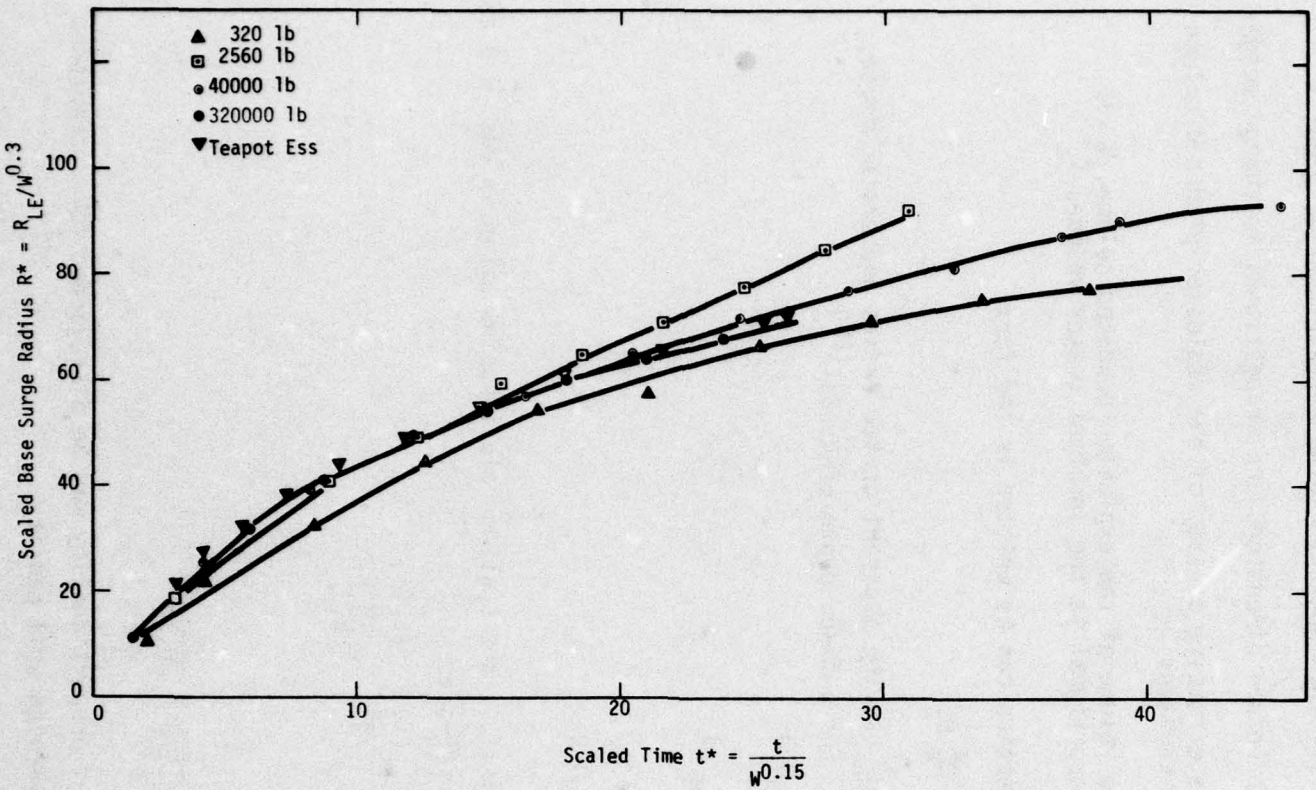

Figure 4.8. Scaled Base Surge Growth for Scaled Depth-of Burial 64.5 ft/$kt^{1/3}$.

sec/kt$^{0.15}$. The experimental data also indicate that the column dimensions for the 320 pound charge are not proportional to Teapot Ess as shown below

	320 lb HE	Teapot Ess
$\frac{\text{Maximum column height}}{\text{Maximum column diameter}}$	0.975	0.432

Thus, at least for this scaled depth, the 320 pound charge does not appear to be similar to Teapot Ess. The results of Figure 4.8 indicate that the large-yield charges appear to be similar to the nuclear data, but since the maximum column dimensions were not reported, it is not possible to establish this equivalence.

At the present time, only limited HE data have been obtained to supplement the nuclear data in the depth-of-burial regime of interest. The data required include the measured radial growth of the base surge cloud and the maximum dimensions of the explosion-produced column. The only data that have been obtained so far are for the 320 pound charges fired in dry clay at the Dugway Proving Ground[7]. As indicated above, these data may not be similar to the nuclear data. Table 4.3, for example, shows the ratios of column to crater volumes to be completely different from those observed in the nuclear tests. Only near the SEDAN depth of burst is the HE ratio compatible with the nuclear value.

Data obtained from the underground explosion tests in soil at the Dugway Proving Ground[7] for dry sand, dry clay and wet clay are plotted in Figure 4.9. These are the only data that have been obtained which indicate the sensitivity of the base surge growth to soil composition and soil moisture content. These data are not adequate for a qualitative description of the soil dependency, but they do indicate trends. It can be seen that a well developed base surge forms in each of the soils, with the largest base surge forming in dry sand and the smallest forming in wet clay. There is no

Table 4.3. Correlation of Column and Crater Volumes

HE SHOT NUMBER	OR	NUCLEAR SHOT	Depth of Burst ($ft/kt^{1/3}$)	$\frac{V_s}{V_a}$
302		—	0	37.3
—		JANGLE U	16.0	131
303		—	33.9	8.7
—		ESS	61.4	108
304		—	64.5	17.8
305		—	128.5	16.0
—		SEDAN	136.8	17.0
306		—	258.3	2.6
307		—	386.8	0.46

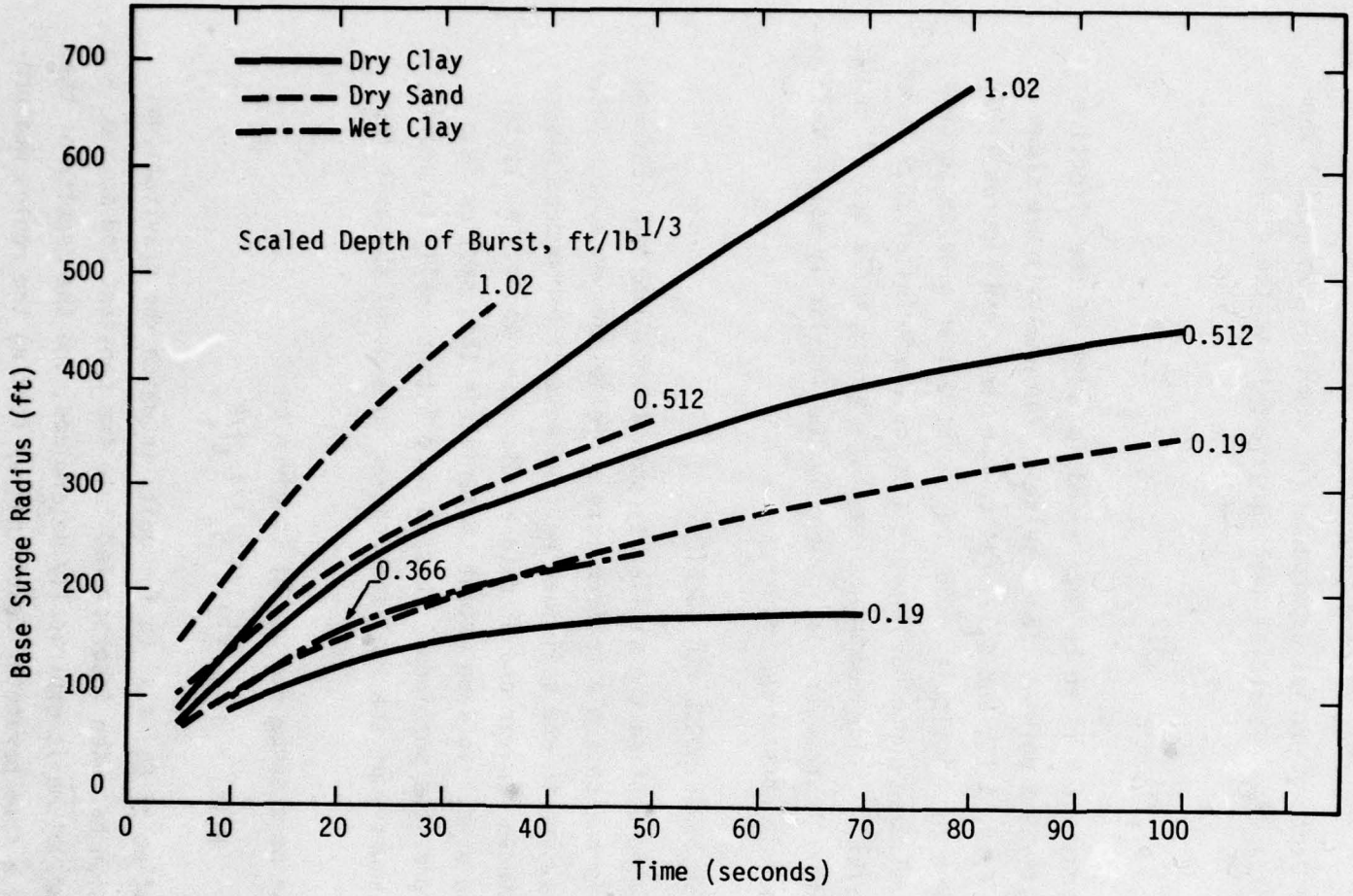

Figure 4.9. Base Surge Growth for 320 lb Charges in Dry Clay, Dry Sand and Wet Clay.

reason to expect this to be indicative of the soil dependence for nuclear shots. At the present time, the column dimensions for the shots fired in dry sand and wet clay are not known.

The depth-of-burial dependence for dry clay was established by fitting the measured radial base surge growth to the similarity solution,

$$R_{LE}(t) = K \cdot t^{1/2}$$

where the constant K is to be determined in terms of the effective column density and volume. The results of the analysis are shown in Figures 4.10, 4.11, and 4.12. It can be seen from Figures 4.10 and 4.11 that the similarity solution is valid over a major portion of the radial base surge development for scaled depths of 23.9 ft/kt$^{1/3}$ and 64.5 ft/kt$^{1/3}$. The measured base surge growth for a scaled depth of 128.5 ft/kt$^{1/3}$,however, does not obey the similarity solution (i.e., K is not nearly constant).

4.4 BASE SURGE MODEL FOR DELFIC

Having applied the similarity solution to Jangle U, Ess and Sedan, it is now possible to formulate a preliminary model for base surge radial growth and soil loading. Because of pronounced discrepancies between nuclear and HE data as discussed above, the latter will not be used. To some extent, material in this section is a repeat of previous sections. This is done intentionally to provide a unified summary of the analysis leading to a model suitable for DELFIC.

The base surge radius, R, is given by

$$R(ft) = 3.57 \left(\frac{\Delta\rho}{\rho_s}\right)^{1/4} V_s^{1/4} t^{1/2},$$

an adaptation of Eq. 4.3 to fps units in which the gravitational acceleration has been incorporated into the constant and $\Delta\rho = \rho_s - \rho_o$. The column volume is empirically determined, and the density of the column is a free parameter determined by fitting the radius measure-

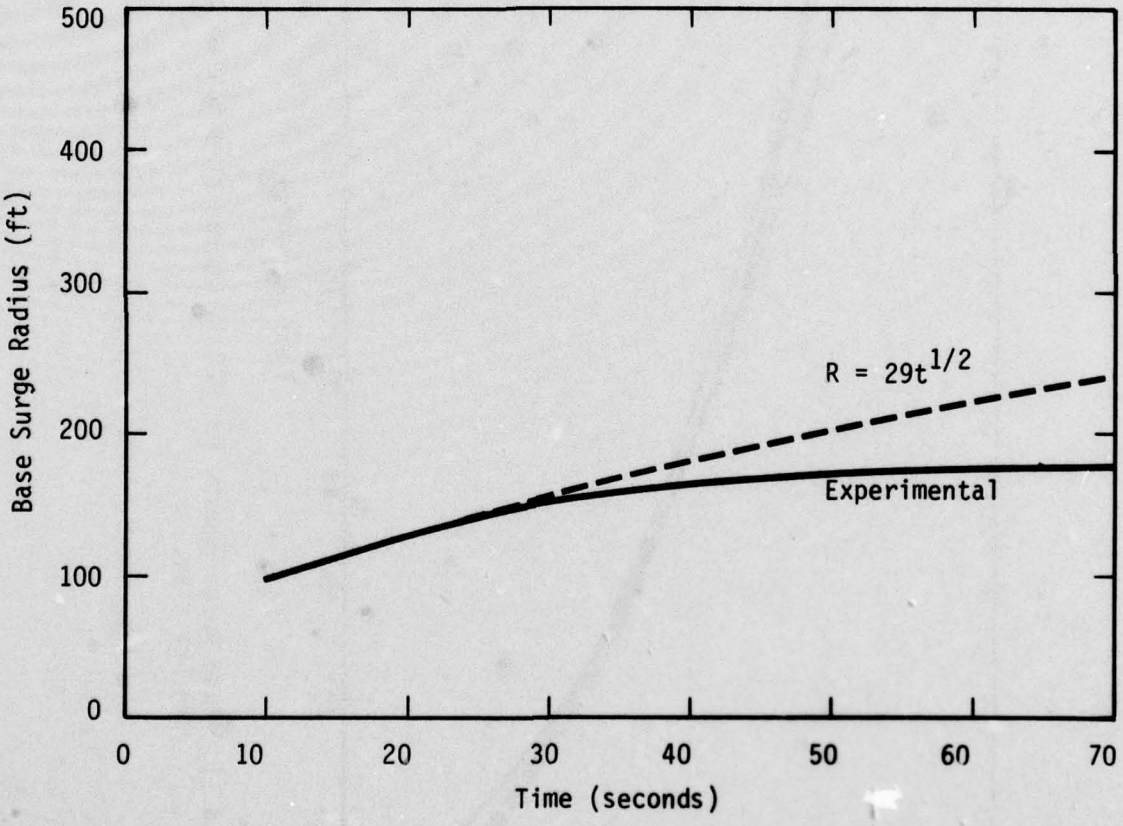

Figure 4.10. Base Surge Growth for 320 lb Charge at a Scaled Depth of 23.9 ft/kt$^{1/3}$ in Dry Clay.

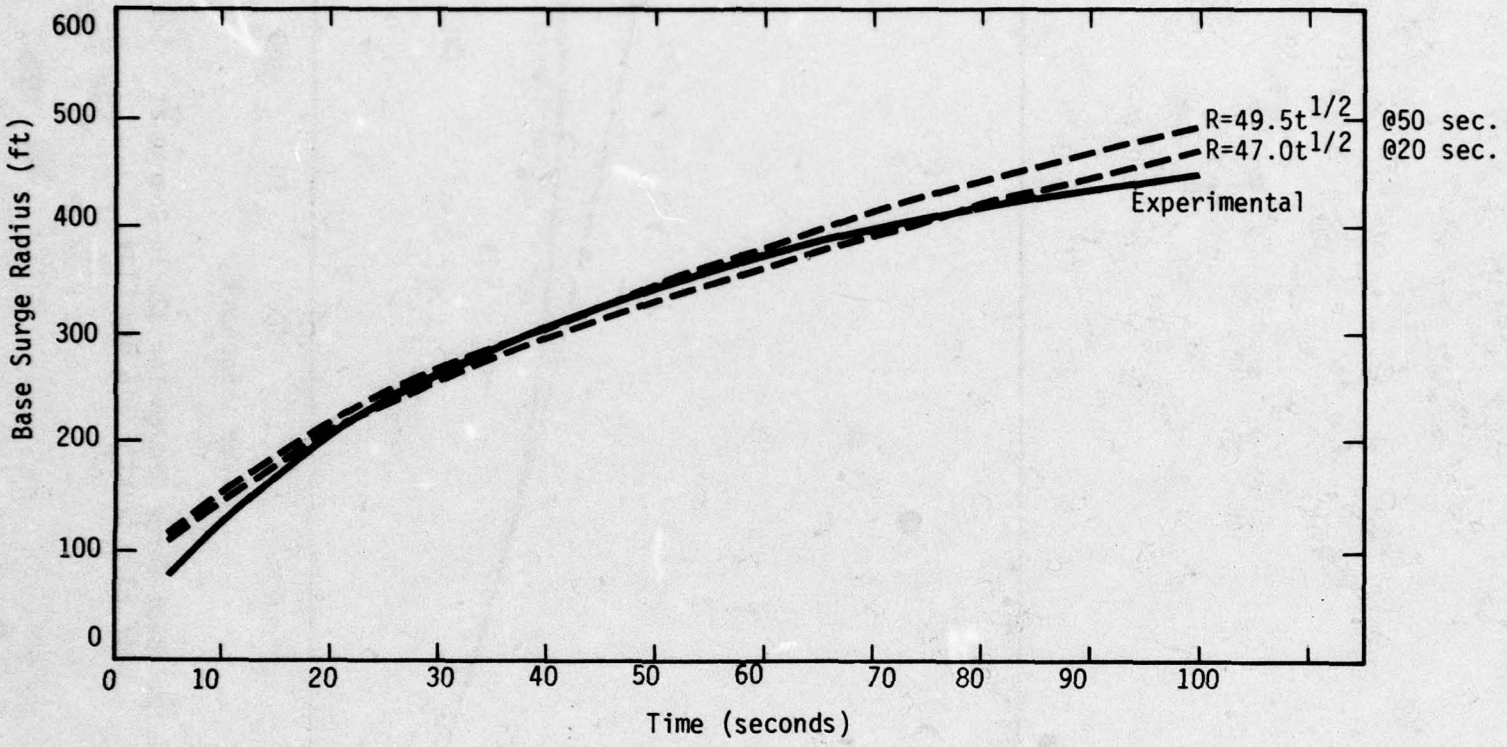

Figure 4.11. Base Surge Growth for 320 lb Charge at a Scaled Depth of 64.5 ft/kt$^{1/3}$ in Dry Clay.

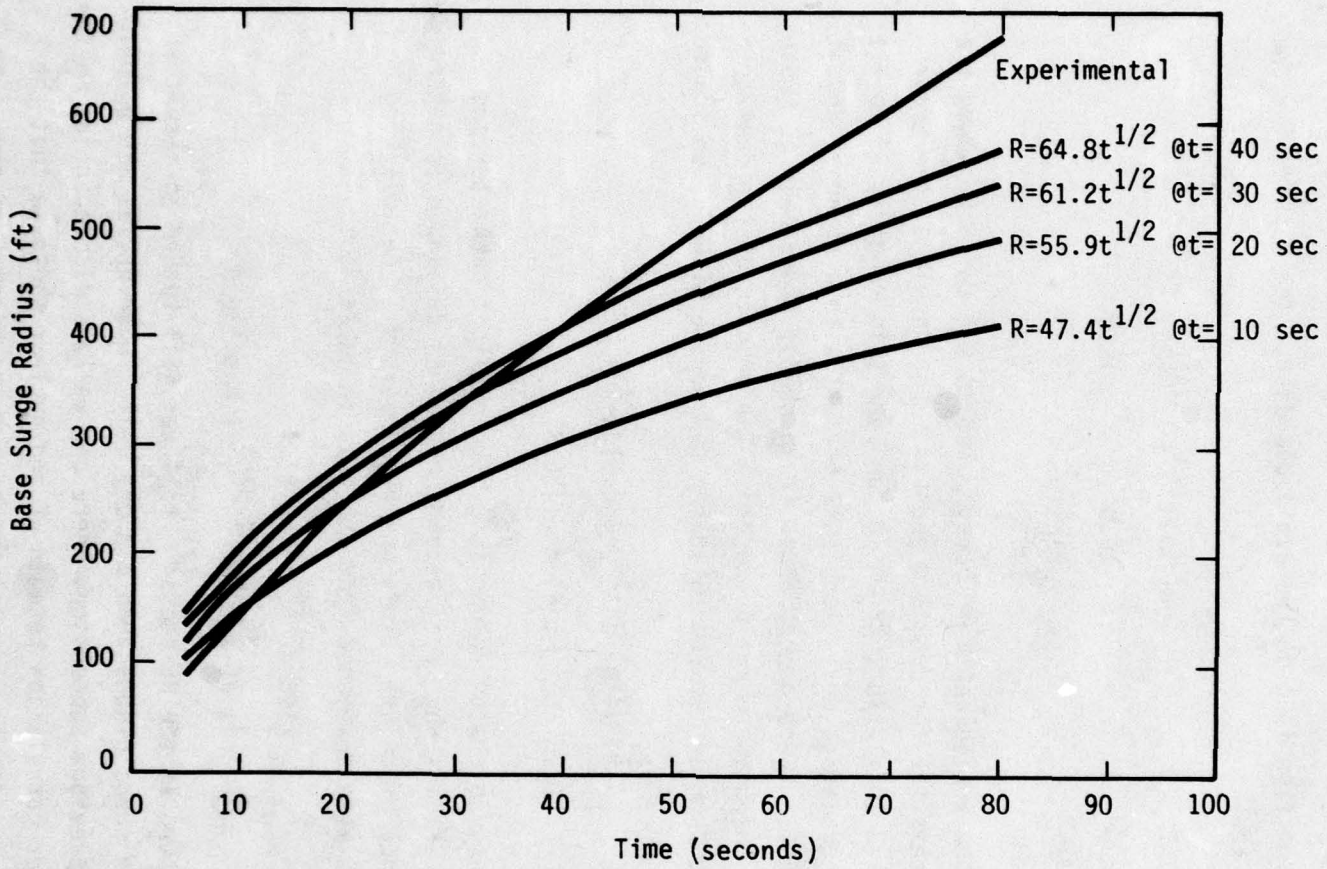

Figure 4.12. Base Surge Growth for 320 lb Charge at a Scaled Depth of 128.5 ft/kt$^{1/3}$ in Dry Clay.

ments to the above expression. For each shot

$$\frac{\Delta\rho}{\rho_s} = \frac{1}{n}\sum_{i=1}^{n} \frac{R^4_{meas}}{t^2} \cdot \frac{1}{(3.57)^4 V_s}$$

where the summation is over the available data. The results for the density fit are

SHOT	$d(ft/kt^{1/3})$	$\Delta\rho/\rho_s$
Uncle	16.0	0.06
Ess	61.4	0.53
Sedan	136.8	0.61

where d is the scaled depth of burst. Tables 4.1 and 4.2 showed the results of this fit for Jangle U and Ess. For Jangle U, the error ranges from -8 to +17 percent while for Ess, this range is -3 to +11 percent. The average deviation is +1 percent with a standard deviation of $\pm$ 7 percent. These error ranges are probably comparable to those inherent in the measurement procedure. The results of the density fitting procedure define the following dependense of $\Delta\rho/\rho_s$ on scaled depth:

$$f = \frac{\Delta\rho}{\rho_s} = \begin{cases} 7.93 \times 10^{-4} d^{1.58}, & 0<d<61.4 \\ 0.257\, d^{.176}, & 61.4<d<136.8 \end{cases}$$

Because crater volume is a more explicit parameter and because it contains the soil dependence, it is desirable to determine the dependence of column volume on crater volume. The following correlations were developed from the data in Table 4.3:

$$h = \frac{V_s}{V_a} = \begin{cases} 195\, d^{-.144}, & 0<d<61.4 \\ 1.45 \times 10^6\, d^{-2.31}, & 61.4<d<136.8 \end{cases}$$

It was observed at the HE tests[7] that wet soil tended to result in smaller base surge clouds than did dry soil. However, as was pointed out in the previous subsection, there are serious discrepancies in the column/crater correlation between HE and nuclear shots so that the effect of wet soils in reducing the base surge dimensions cannot be assumed to apply for the nuclear case. Until more information is available, the above correlation will be assumed for all soils.

The formulation of base surge radial growth using the similarity solution does not provide for a maximum radius, so that growth must be artificially terminated. The time at which the radius reaches its maximum will be assumed to be that corresponding to the last measurement. This time will be converted to a scaled time as follows:

$$t^* = \left(\frac{\Delta\rho}{\rho_s}\right)^{\frac{1}{2}} V_s^{-1/6}\, t$$

For Jangle-U, Ess and Sedan, the values of t^*_{max} are 1.98, 6.87, and 7.39, respectively. As a function of d:

$$t^*_{max} = \begin{cases} .152\ d^{.925}, & 0 < d < 61.4 \\ 4.72\ d^{.092}, & 61.4 < d < 136.8 \end{cases}$$

The maximum base surge radius is then given by

$$R_{max} = 3.57\ (t^*_{max})^{1/2} (h\ V_a)^{1/3}$$

Combining of the dependencies of t^*_{max} and h gives

$$R_{max} = \begin{cases} 8.07\ d^{.415}\ V_a^{1/3}, & 0 < d < 61.4 \\ 877\ d^{-.724}\ V_a^{1/3}, & 61.4 < d < 136.8 \end{cases}$$

where V_a obviously depends on both yield and the scaled depth.

The temporal dependence of the base surge radius is expressed as follows:

$$R = R_{max} \left(\frac{t^*}{t^*_{max}}\right)^{\frac{1}{2}}, \quad t^* < t^*_{max}$$

Figure 4.13 is provided as a comparison of the model described above with what is used in KDFOC[3] and what has been developed by the Nuclear Cratering Group[9]. The ordinate is the maximum base surge radius scaled to 1 kt and the abscissa is scaled depth of burst. The crater volume for the similarity solution is taken from EM-1[11] for dry soil. Also shown are the scaled maximum radii for the three shots used in calibrating the model. The best agreement with the data comes from the model presented here.

As was discussed previously, the similarity solution does not account for turbulent mixing and hence does not give good agreement with the maximum base surge height measurements. The simplest approach is to develop a correlation with the maximum radius. Figure 4.14 shows a variety of data from which this correlation can be developed. Two curves are shown, one for nuclear and one for HE. For the latter, the height tends to be only 25 to 35 percent of what would be expected for a nuclear shot with the same radius. The nuclear correlation thus will be used without regard for the HE data.

The fit is

$$H_{max}(ft) = 8.8\, R_{max}^{0.65}$$

where R_{max} is the maximum base surge radius in feet.

The final specification required for the base surge is the soil burden. The total mass is given by

$$M = V_s \rho_s$$

Subtracting out the air leaves

$$M_B = V_s \Delta\rho = V_s \left(\frac{\Delta\rho/\rho_s}{1-\Delta\rho/\rho_s} \right) \rho_o$$

Using the correlations developed above, M_B is expressed in terms of the crater volume as

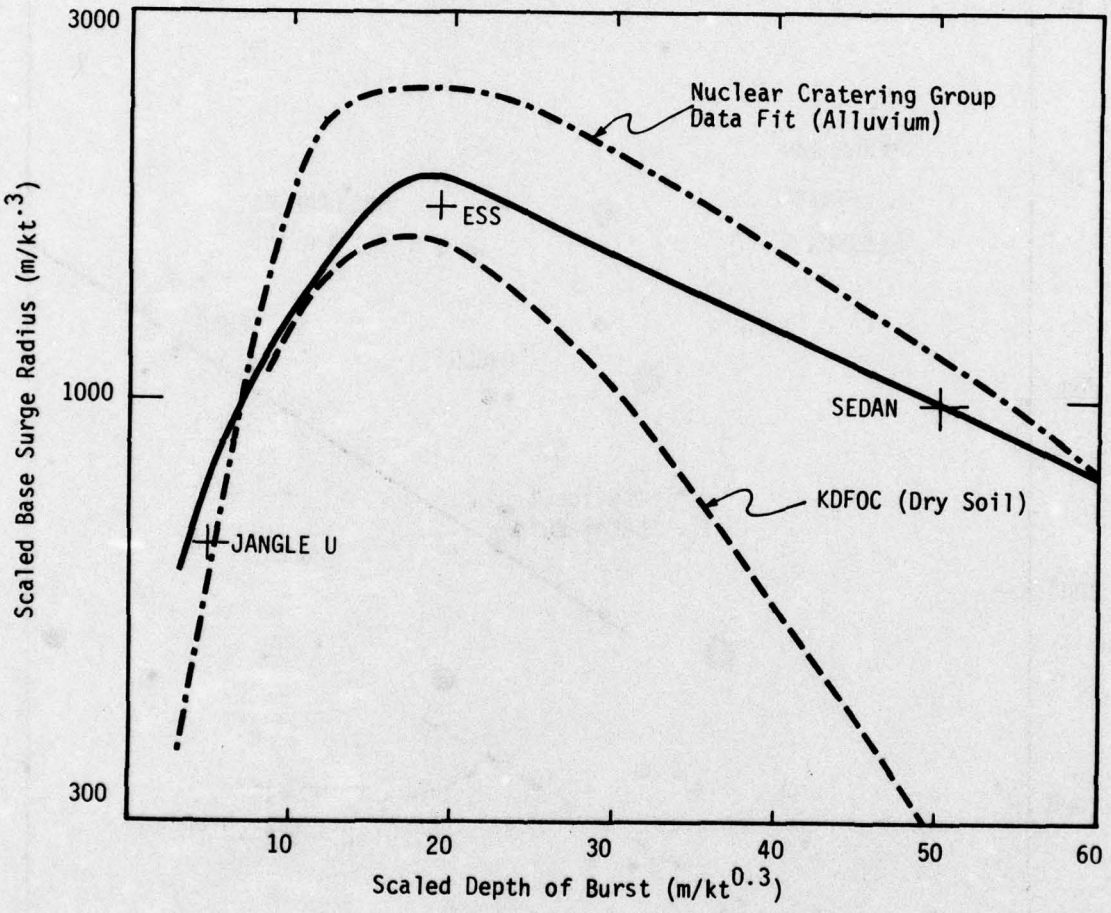

Figure 4.13. Comparison of Various Models of Base Surge Radius

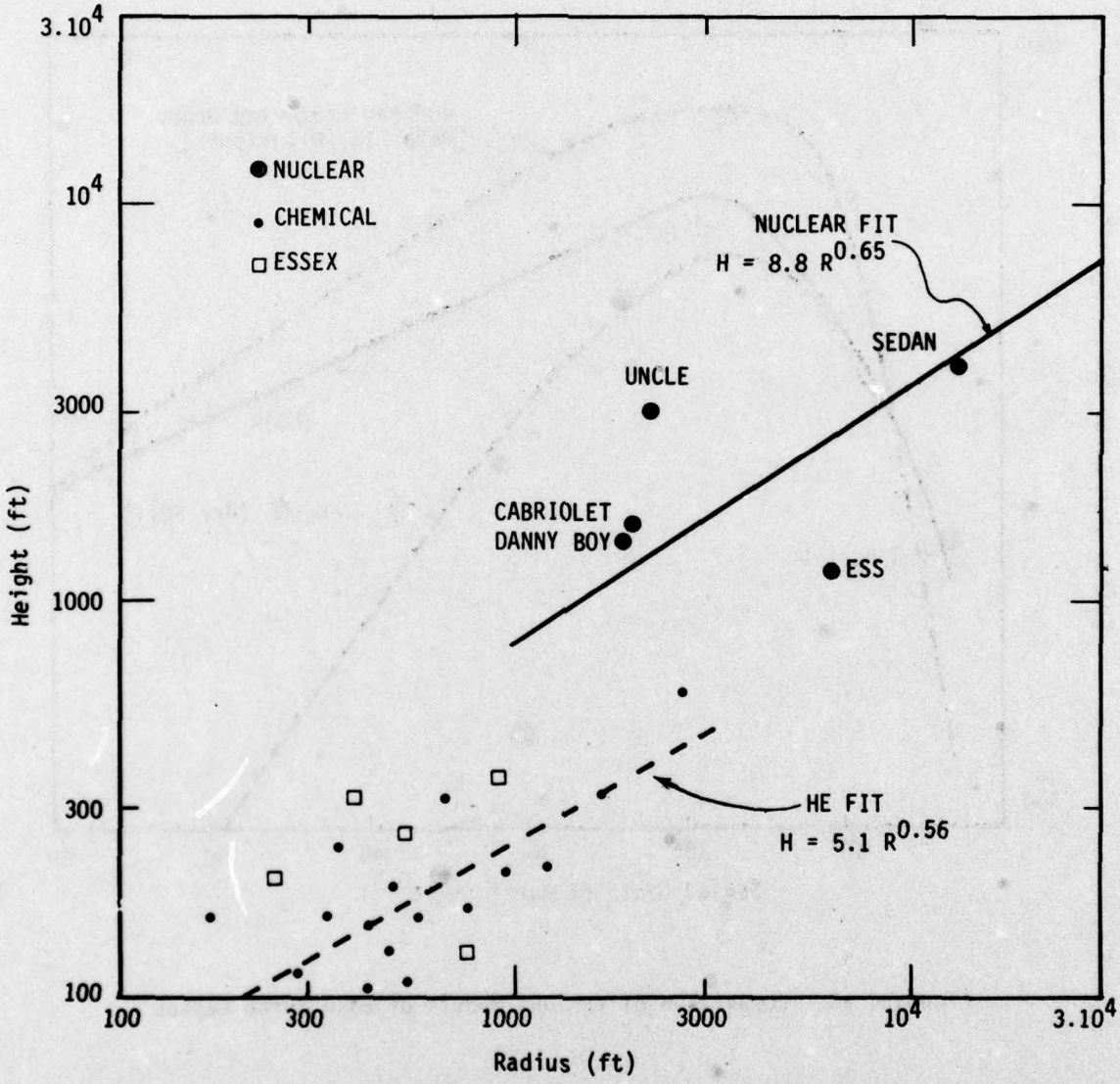

Figure 4.14. Correlation of Base Surge Height and Radius.

$$M_B = \rho_o \frac{f}{1-f} \cdot h \cdot V_a$$

Assuming an ambient air density of 1.29×10^{-3} gm/cm^3 (.081 lbs/ft^3) and combining the expressions for f and h gives

$$M_B(\text{lbs}) = \begin{cases} \dfrac{.0125\ V_a d^{1.44}}{1-7.93\times10^{-4} d^{1.58}}, & 0 < d < 61.4 \\ \dfrac{3.02\times10^{4}\ V_a d^{-2.13}}{1-7.93\times10^{-4} d^{1.58}}, & 61.4 < d < 136.8 \end{cases}$$

Using a bulk density (ρ_a) of 1.9 and 1.5 gm/cc for dry and wet soils (cf the Appendix), respectively, results in the following relationships of base surge soil loading as a ratio of crater mass (i.e., $M_B/\rho_a V_a$).

scaled burst depth	DRY	WET
$0 < d < 61.4$	$\dfrac{1.06\times10^{-4} d^{1.44}}{1-7.93\times10^{-4} d^{1.58}}$	$\dfrac{1.34\times10^{-4} d^{1.44}}{1-7.93\times10^{-4} d^{1.58}}$
$61.4 < d < 136.8$	$\dfrac{255 d^{-2.13}}{1-7.93\times10^{-4} d^{1.58}}$	$\dfrac{323 d^{-2.13}}{1-7.93\times10^{-4} d^{1.58}}$

This completes the specification of the base surge dimensions and soil loading.

4.5 REFERENCES

1. V.G. Khorguani, "The Character and Settling Velocity for a System of Equal Size Particles", Atmospheric and Ocean Physics, Vol. 2, 234 (1966).

2. G.A. Young and M.L. Milligan, "Operation Jangle, Project 1(9)b, Base Surge Analysis of Nuclear Tests", WT-390, U.S. Naval Ordnance Laboratory, June 1952.

3. M.L. Milligan and G.A. Young, "Operation Teapot - Underground Shot Base Surge Analysis", U.S. Naval Ordnance Laboratory, NAVORD Report 4153, January 1953.

4. Project SEDAN, Project Manager's Report, Plowshare Program, May 1963.

5. M.D. Nordyke and M.M. Williamson, SEDAN Event, Lawrence Radiation Laboratory, Report PNE-242F, April 1965.

6. O.G. Tietjens, Fundamentals of Hydro- and Aeromechanics, Dover Publications, Inc., 1934.

7. G.A. Young, "Operation Jangle, Project 1(9)-4, Base Surge Analysis-HE Tests", WT-339, U.S. Naval Ordnance Laboratory, November 1951.

8. J.B. Knox, et al., "KDFOC" A Computer Program to Calculate Fallout from Underground and Land Surface Nuclear Explosions," Lawrence Livermore Laboratory, Report UCRL-51179, (Unpublished).

9. W.C. Day, "Cloud Dimensions for Cratering Explosions," U.S. Army Engineer Nuclear Cratering Group, Technical Memorandum NCG/TM66-8, September 1966.

10. Defense Nuclear Agency, "Capabilities of Nuclear Weapons," Philip J. Dolan, Ed., (Unpublished).

SECTION 5

VENT FRACTION AND ACTIVITY PARTITION

The previous sections have presented results of the analyses defining the characteristics (in particular, dimensions and soil loading) of the main and base surge clouds as functions of yield, depth of burst and soil. This section is devoted to the determination of the total activity in the fallout pattern, or vent fraction, and the partition of this activity between the two clouds.

5.1 VENT FRACTION

With present capabilities, it is not possible to develop a theoretical model for vent fraction as a function of depth of burst. Thus this dependence is based on analysis of fallout patterns from subsurface tests. The parameter of interest is the so-called K-factor, which has units of R/HR (at 1 hr) kt^{-1} mi^2. For a nominal 1 kt surface burst, for example, if the fallout were uniformly spread over a smooth plane, 1 mile square in area, the one hour dose rate would be 3380. Typically, a factor of 0.74 is incorporated to account for terrain roughness.[1] For a given subsurface test, measurements of radioactivity are made at a finite number of locations, with the resulting intensities corrected to 1 hour after burst. Iso-dose-rate contours are then generated and the actual K-factor is determined as

$$K = \frac{1}{W} \int I \cdot dA$$

where I(A) is the one-hour dose rate corresponding to an increment of area dA. Vent fraction is then the value of this integral divided by the surface burst K-factor for the yield W(kt). Because there is often only limited data and also because of the uncertainty inherent in extropolating a measurement back in time to 1 hour, there is considerable disagreement within the fallout community about the dependence of vent fraction on depth of burst. Table 5.1 provides a

comparison of values based on analys ; by Tompkins[2] and Knox[1]. For surface or near surface shots, there is reasonable agreement, as evidenced by the Johnny Boy comparison. However, Knox's values are about 45 percent lower than Tompkins' for three shots in alluvium (Jangle U, Ess and Sedan) that range in scaled depth of burst from 4 to 40 $m/kt^{1/3}$. For Danny Boy, which is as deep as SEDAN but in basalt instead of alluvium, Knox's value is a factor of four lower than Tompkins'.

It is beyond the scope of this study to recommend one set of vent fraction values over the other. A detailed exercise of DELFIC, once it has a subsurface capability, might be the best approach toward resolving the differences.

5.2 ACTIVITY PARTITION

The simplest algorithm for dividing the total vented activity between main and base surge clouds is on a mass basis. c.e.,

$$A_m = V.F. \left(\frac{M_m}{M_m + M_B}\right)$$

$$A_B = V.F. \left(1 - A_m\right)$$

where A_m is the activity in the main cloud, VF is the vent fraction. The fraction of vented activity in the main cloud is then just the fraction of lofted soil in the main cloud. As discussed in the previous sections, both the soil burden in the main cloud and that in the base surge were expressed in terms of apparent crater mass. It is then a simple matter to determine the main cloud fraction of lofted soil. Table 5.2 provides these fractions for dry and wet soils.

Figure 5.1 shows the dependence of the main cloud soil fraction on scaled depth of burst for dry soil (see Table 5.2). Also shown in the curve used in KDFOC for the main cloud activity fraction. Three data points are shown for Jangle U, Ess, and Sedan respectively.

TABLE 5.1

COMPARISON OF VENT FRACTION

Shot	Scaled Depth of Burst $m/kt^{1/3}$	Vent Fraction	
		Tompkins	Knox
JOHNNY BOY	0.73	.68	.52
JANGLE U	4.88	.99	.56
TEAPOT ESS	18.7	.75	.41
SEDAN	41.8	.34	.18
DANNY BOY	44.7	.16	.04
NEPTUNE	61.6	.0014	.0032

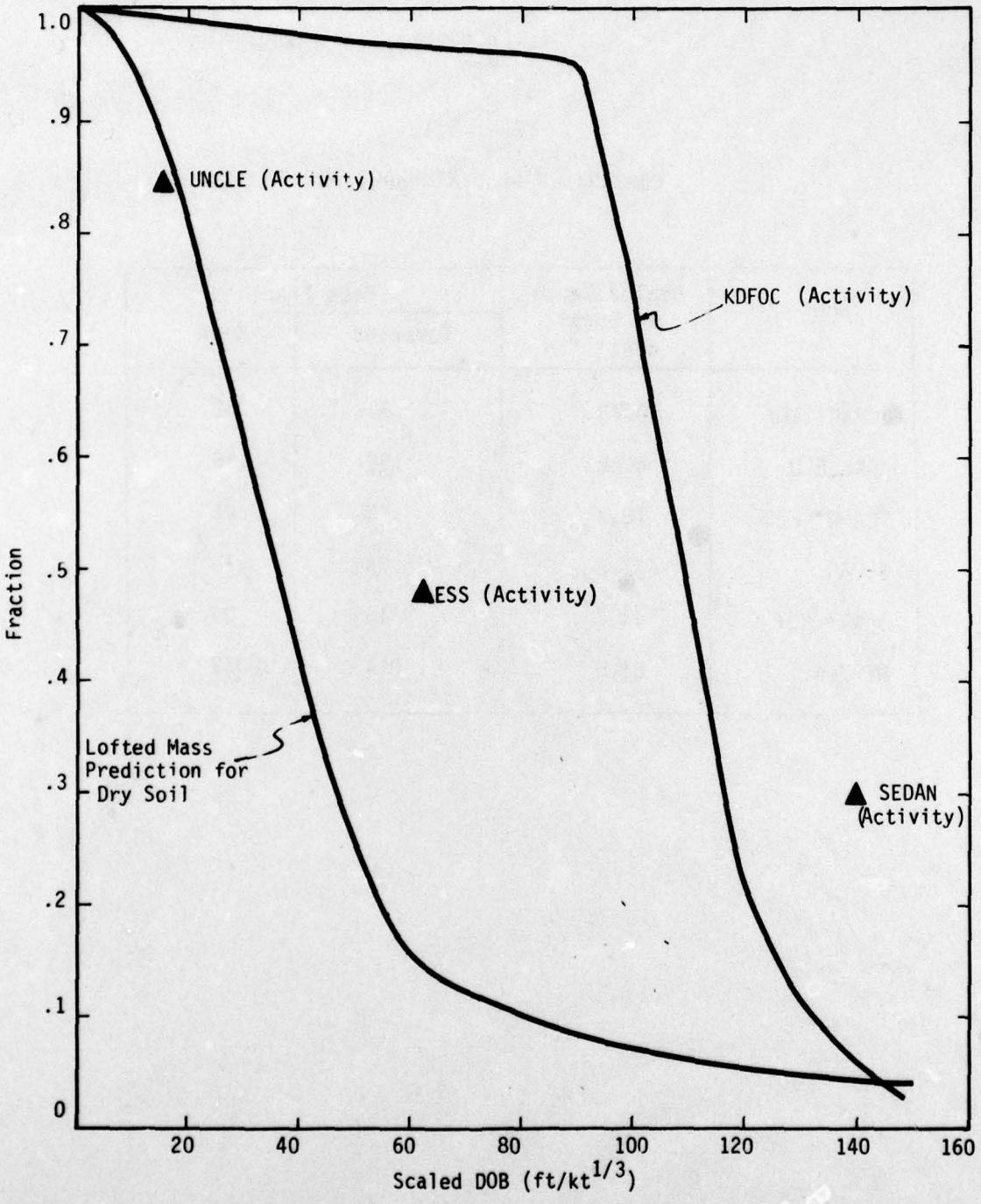

Figure 5.1. Fraction of Lofted Mass and Vented Activity in Main Cloud.

TABLE 5.2

SOIL BURDEN IN MAIN AND BASE SURGE CLOUDS

Scaled Depth of Burst $\frac{d}{ft/kt^{1/3}}$	$\frac{M_m(d)}{M_a(d)}$		$\frac{M_B(d)}{M_a(d)}$		$\frac{M_m(d)}{M_m + M_B}$	
	DRY	WET	DRY	WET	DRY	WET
0	.140	.140	0	0	1.0	1.0
10	.134	.135	.009	.011	.937	.925
20	.101	.108	.023	.029	.815	.788
30	.068	.079	.042	.053	.618	.599
40	.045	.058	.063	.080	.417	.420
50	.031	.042	.087	.110	.263	.276
60	.020	.031	.113	.143	.150	.178
70	.014	.022	.094	.119	.130	.156
80	.009	.016	.074	.093	.108	.147
90	.006	.012	.060	.076	.091	.136
100	.004	.009	.049	.063	.076	.125
120	.002	.005	.035	.045	.054	.100
150	.001	.002	.024	.030	.040	.063

NOTE: M_m, M_B, M_a = soil mass in main cloud, base surge and apparent crater

As an example of how the main cloud activity fraction is calculated from an observed fallout pattern, consider ESS. The ground zero width data activity measurements resulted in the following fit[3]:

$$\dot{D}(r) = 1200\ e^{-r^2/7.9}$$

where $\dot{D}(r)$ is the one hour dose rate at a range, r, in kft. The ground zero width data is assumed to be due only to fallout from the base surge. This equation is then integrated from the radial throwout extent of 2 kft to the base surge radius of 8 kft. The K-factor integral is:

$$K_B = \frac{1}{W}\int \pi 2\ rdr\ \dot{D}(r)$$

Converting area units from kft^2 to $miles^2$ results in

$$K_B = 536\ R/Hr\ kt^{-1}\ mi^2$$

Using Knox's vent fraction value of 0.41 from Table 5.1 the total K value is

$$K = 0.41 \times 3380 \times 0.74 = 1025\ R/Hr\ kt^{-1}\ mi^2$$

Thus the fraction in the base surge is 0.52, and the fraction in the main cloud is 0.48. Note that the predicted mass fraction as shown in Figure 5.1 is about 0.15 at the ESS depth, or a factor of three lower than the empirically determined activity fraction. This suggests that the simple assumption that activity correlates directly to mass is not viable. In support of this, an analysis[4] of fallout samples obtained from the ESS shot indicated that the specific activity (in millicuries per gram) from a sample obtained near ground zero (where the base surge predominated) was a factor of about 2 lower than that for a downwind sample (where both the base surge and main cloud contributed fallout). More precisely, the ground zero and downwind specific

activities (α) were 2.3 and 4.8 mc/gm. Assume the first value to be representative of the entire base surge so that

$$\alpha_B = 2.3 \text{ mc/gm}$$

Since the downwind sample is an undetermined mix of base surge and main cloud contributions, it is not possible to assign a corresponding representative value to the main cloud specific activity, α_m. In other words, the downwind sample has a specific activity represented by:

$$\alpha_D = \frac{\alpha_B m_B + \alpha_m m_m}{m_m + m_B} = 4.8 \text{ mc/gm}$$

where α_B is given above and the mass contributions m_m and m_B pertain to that sample only.

Returning now to Figure 5.1, the relationship between main cloud mass and activity fractions F and F_A is as follows:

$$F_A = \frac{A_m}{A_m + A_B} = \frac{\alpha_m M_m}{\alpha_m M_m + \alpha_B M_B} = \frac{F\alpha_m}{F\alpha_m + (1-F)\alpha_B} .$$

The value of α_B is given above, but that for α_m can only be inferred from the downwind measurement. Using the predicted value of 0.15 for F, there are several possibilities:

a.) if the base surge did not contribute to the downwind sample, then $\alpha_B = \alpha_D$ and $F_A = 0.27$, roughly half the observed value. However, considering the size of the base surge and the close-in location of the downwind sample, it is not likely that there was no base surge contribution

b.) if the main cloud and base surge contributions are equal (i.e., $m_m = m_B$), then $\alpha_m = 7.3$ mc/gm and F_A is 0.36, or 75 percent of that observed

c.) in order for the predicted mass fraction and the observed activity fraction to be consistent, the required value of α_m is 12.0 mc/gm, implying that the main cloud contributed roughly one-third as much as the base surge to the mass of the downwind sample.

Both items b and c above are plausible assumptions. The comparison of specific activity data from ground zero and downwind samples leads one to expect the main cloud mass fraction to be no more than half the activity fraction. This is indeed predicted.

Once DELFIC has been modified to handle subsurface bursts, a detailed calculation of the predicted mass fractions from each of the clouds at specific sample locations would be desirable in establishing specific activity differences between main and base surge clouds.

5.3 INDUCED ACTIVITY

For certain types of nuclear devices, the contribution of induced activity to fallout may be significant. By induced activity is meant the activation of soil in the immediate vicinity of the explosion by neutrons. In addition to device type, an important specification is the soil itself. The water in the soil absorbs neutrons without undergoing subsequent radioactive decay. However, certain elements, because of their capture cross section and decay half-life, can contribute to the total induced activity much more strongly than their mass fraction might indicate. The key parameters then are:

a) device type and neutron energy spectrum

b) soil composition

c) depth of burst and hence the fraction of neutrons captured in soil entrained into either the main cloud or base surge cloud.

In the present version of DELFIC, 17 percent of the neutrons are assumed to be captured for a surface burst. An investigation[5] based on numerical calculations showed that the fraction captured by soil that was later entrained into the cloud depended on yield and energy spectrum. High energy neutrons (14 Mev) were twice as likely to be captured in entrained soil as 0.5 Mev neutrons. This, however, applied to surface bursts where air scatter is important.

Recently a calculation[6] was performed to determine the extent to which neutrons contribute to the initial nuclear radiation from a shallow-buried weapon. It was found that soil is ejected from the crater before some of the neutrons have been thermalized (slowed down) to the point where they could be captured and that there is some fraction of neutrons captured by the soil above the ground plane. More specifically, the calculation was for 1 kt at a depth of burst of 1 m. The fraction of neutrons captured below ground was 36 percent, while 7 percent were captured by soil above ground, for a total of 43 percent. Unfortunately, it is not known what fraction of the total activated soil should be attributed to the main and base surge clouds vis a vis crater ejecta and fallback. Since the mean free path of neutrons in soil is very short (i.e., flux is attenuated to 1 percent within one meter), one would expect that the soil activated below ground is co-located with the fission debris gases. A further assumption that appears reasonable is that this component of the activated soil will be dispersed with the fission debris and that its vent fraction is the same as for the fission debris.

Unfortunately, because the calculation in Reference 6 was performed at only one depth of burst, it is not possible to determine at what depth of burst all of the neutrons are captured in soil. An estimate, however, can be made based on the strong shock solution for soils of γ=1.4. The shock radius, R_s, is dependent on time (in seconds) as follows:

$$R_s(m) = 86.8 \left(\frac{W(kt)}{\rho(gm/cc)}\right)^{1/5} t^{2/5}.$$

The time by which the neutrons will have been thermalized and captured is approximately 1 msec. If the depth of burst is equal to or greater than the shock radius at this time, then it can be assumed that all of the neutrons have been captured in soil. For dry soil with a density of 1.9 gm/cc, this depth of burst is 4.8 m at 1 kt and 12.1 m at 100 kt. Thus the fraction captured, F_c, is

$$F_c = \begin{matrix} 1.0 \text{ @ DOB} = 4.8 \text{ m } W^{1/5} \\ 0.43 \text{ @ DOB} = 1 \text{ m } W^{1/5} \end{matrix}$$

where the yield scaling is taken to be the same for both estimates. For intermediate depths, linear interpolation can be used, so that

$$F_c = 0.28 + 0.15 \text{ DOB } W^{-1/5}$$

For wet soils in which the density is 1.5 gm/cc, the corresponding expression may be easily derived.

5.4 REFERENCES

1.) J. Knox, et al., "Radioactivity Released from Underground Nuclear Detonations: Source, Transport, Diffusion and Deposition," UCRL-50230, Rev. 1, Lawrence Livermore Laboratory, March 1970.

2.) R. Tompkins, "Effect of Depth of Burial on Fallout from Atomic Demolition Munitions," BRL-MR-2317, U.S. Army Ballistic Research Laboratories, Aug. 1973.

3.) Weapons Effects Handbook for the Long Range Research and Development Program, Science Applications, Inc., Feb., 1973.

4.) M. Milligan and G. Young, "Operation Teapot - Underground Shot Base Surge Analysis," NAVORD Report 4153, U.S. Naval Ordnance Laboratory, Jan. 1953.

5.) J. McGahan, et al., "Sensitivity of Fallout Predictions to Initial Conditions and Model Assumptions," DNA 3439F, Science Applications, Inc., Dec. 1974.

6.) W. Scott et al., "Lofted Neutron Doses from a Shallow Buried Munition," Draft Report, SAI-77-137-LJ, Science Applications, Inc., (Unpublished).

Section 6

CONCLUSIONS

The work reported on in the previous sections is an attempt to draw on current understanding of the phenomenology of fallout from subsurface bursts. Specifically, models have been developed for:

a.) main cloud effective yield and soil loading

b.) base surge radial growth, height and soil loading with a dependence on soil density

c.) induced activity

Important parameters that have not been modeled include vent fraction and the partition of activity between the main and base surge clouds.

6.1 SUMMARY

This section presents the major conclusions of the study.

a.) DELFIC's present formulation of the main cloud initial conditions is very sensitive to the soil temperature and loading. If the temperature is too high, there will not be enough energy to drive the cloud rise.

b.) An effective yield model, dependent on depth of burst (DOB) and the bulk density of the soil, has been presented and found to adequately describe the decrease in stabilized main cloud height as DOB increases. When used in conjunction with DELFIC's dynamic cloud rise model to predict observed cloud dimensions and height, it is expected that soil temperature can be determined.

c.) This effective yield, in conjunction with the crater volume dependence on DOB and soil, can be used to determine the soil loading of the main cloud.

d.) A review of the vent fractions determined from the ESSEX series of HE tests indicates that there are several aspects which make the analogy with the nuclear case difficult. Among these is that an HE test is likely to have different equivalent nuclear yields for cratering and base surge formation as opposed to venting and the definition of the main cloud. Further theoretical investigations are required in order to assess how HE data such as ESSEX may be used to enhance the limited nuclear data base.

e.) A model based on a similarity solution was developed for the radial growth of the base surge, with the free parameter being the column soil density. The error in the model when compared with measurements of the radius versus time for 3 nuclear shots averaged below 10 percent. The model does not account for turbulent mixing and hence is inadequate in predicting base surge height; instead an empirical correlation was developed with radius. Column density and correlation with crater volume are provided as functions of DOB. Since mass is assumed to be conserved in the developing base surge, the soil loading can be determined directly. There were several areas of similar effects, as well as differences, between HE and nuclear data in developing the required correlations.

f.) The predicted mass partition between the main and base surge clouds indicates that activity is not directly proportional to mass. This is supported by specific activity measurements from the Teapot Ess shot, where the specific activity was at least a factor of 2 lower for base surge fallout than that due to the main cloud. Thus the models developed for soil loading in the two clouds are not contradicted by the available specific activity data.

g.) Based on a limited calculation of the fraction of neutrons captured by soil, a simple model for the dependence of induced activity on DOB was developed. Refinements are anticipated as more calculations become available.

6.2 RECOMMENDATIONS

As stated in the Introduction of this report, this investigation did not involve an implementation of a subsurface capability in DELFIC. It seems appropriate that this be done with the models that have been developed. To a large extent, the objective of this second phase would be to validate the subsurface modeling and redefine or improve it where necessary. One key area is the level of detail required in describing the base surge. There are essentially two options,the first of which is a simple disk model (with the maximum radius) for which fallout commences at the time growth ceases. The second option is significantly more complex in that trace particles representing the soil loading in the column would be tracked during growth,using a flow field modeled as a jet impinging a flat plate.

As discussed in Section 5, an assessment of the two competing vent fraction algorithms is most properly done in the framework of detailed comparisons of DELFIC predictions with test data. In a similar view, the activity partition is also best determined by regarding it as a somewhat free parameter to be adjusted in an empirical manner.

A final recommendation is to perform a theoretical analysis of the differences evident between HE (i.e., ESSEX) and nuclear vent fraction data so as to develop the correct interpretation of the former in supplementing the nuclear data and providing insight into a potential soil dependence for vent fraction.

APPENDIX

BULK DENSITY FOR VARIOUS SOILS

Table A.1 presents the water content and bulk density for 10 different soils*. Based on this data, the base surge for dry soil assumed a bulk density of 1.9 gm/cc while for wet soil a value of 1.5 gm/cc was used.

Table A.1
Bulk Density and Water Content

DESCRIPTION	WATER CONTENT+	ρ(gm/cm^3)
uniform sand, loose	32	1.89
uniform sand, dense	19	2.09
mixed grain sand, loose	25	1.99
mixed grain sand, dense	16	2.16
glacial till	9	2.32
soft glacial clay	45	1.77
stiff glacial clay	22	2.07
soft slightly organic clay	70	1.58
soft very organic clay	110	1.43
soft bentonite	194	1.27

+ water content when saturated, in percent of dry weight

* Terzaghi and Peck, "Soil Mechanics in Engineering Practice," John Wiley & Sons, New York, NY 1948.

DISTRIBUTION LIST

DEPARTMENT OF DEFENSE

Assistant to the Secretary of Defense
Atomic Energy
ATTN: Executive Assistant

Defense Advanced Rsch. Proj. Agency
ATTN: TIO

Defense Civil Preparedness Agency
ATTN: Postattack Research Division

Defense Documentation Center
12 cy ATTN: DD

Defense Intelligence Agency
ATTN: DB-4D, H. Ward

Defense Nuclear Agency
ATTN: RAAE
ATTN: DDST
ATTN: SPAS
ATTN: STVL
2 cy ATTN: RATN
4 cy ATTN: TITL

Field Command
Defense Nuclear Agency
ATTN: FCPR

Field Command
Defense Nuclear Agency
Livermore Division
ATTN: FCPRL

Joint Strategic Tgt. Planning Staff
ATTN: JPS
ATTN: JLTW
ATTN: JP
ATTN: JL

Under Secretary of Defense for Rsch. & Engrg.
ATTN: Strategic & Space Systems (OS)

DEPARTMENT OF THE ARMY

Deputy Chief of Staff for Rsch. Dev. & Acq.
Department of the Army
ATTN: DAMA-CSS-N

Harry Diamond Laboratories
Department of the Army
ATTN: DELHD-N-NP

U.S. Army Ballistic Research Labs
ATTN: Technical Library
2 cy ATTN: DRDAR-BLB, J. Maloney

U.S. Army Nuclear & Chemical Agency
ATTN: Library

U.S. Army Ordnance & Chemical Ctr. and School
ATTN: H. Whitten

DEPARTMENT OF THE NAVY

U.S. Atlantic Fleet
Department of the Navy
ATTN: Div. 20, Code 22

Naval Surface Weapons Center
White Oak Laboratory
ATTN: Code F31

DEPARTMENT OF THE AIR FORCE

Air Force Systems Command
ATTN: DLS

Air Force Weapons Laboratory
ATTN: DYT
ATTN: SUL

Air Weather Service, MAC
Department of the Air Force
ATTN: AWSAE

Space & Missile Systems Organization
Air Force Systems Command
ATTN: DYAE

DEPARTMENT OF ENERGY

Department of Energy
ATTN: Classified Library
ATTN: H. Hollister

Office of Military Application
Department of Energy
ATTN: R. Engelmann

OTHER GOVERNMENT AGENCY

U.S. Arms Control & Disarmament Agency
ATTN: Ops. & Analysis Div., W. Deemer

DEPARTMENT OF ENERGY CONTRACTORS

Lawrence Livermore Laboratory
University of California
ATTN: L-125, T. Gibson
ATTN: Technical Information Dept. Library
ATTN: L-216, J. Knox
ATTN: L-10, F. Serduke

Sandia Laboratories
ATTN: J. Keizur
ATTN: Orgn. 3141

DEPARTMENT OF DEFENSE CONTRACTORS

Aerospace Corporation
ATTN: R. Strickler

Atmospheric Science Assoc.
ATTN: H. Norment

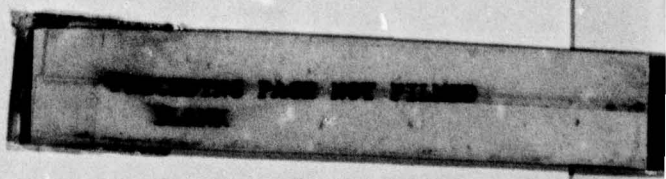

DEPARTMENT OF DEFENSE CONTRACTORS (Continued)

General Electric Co.-TEMPO
Center for Advanced Studies
ATTN: DASIAC

Physics International Company
ATTN: M. McKay

R & D Associates
ATTN: H. Brode
ATTN: C. MacDonald

The Rand Corporation
ATTN: R. Rapp

DEPARTMENT OF DEFENSE CONTRACTORS (Continued)

Science Applications, Inc.
ATTN: D. Hamlin

Science Applications, Inc.
ATTN: J. McGahan
ATTN: R. Latko

SRI International
ATTN: S. Brown
ATTN: P. Dolan